Supplementary information

An oxide-promoted, self-supported Ni_4Mo catalyst for high current density anion exchange membrane water electrolysis

Ariana Serban[a], Meng-Ting Liu[b], Nanjun Chen[a], Hao Ming Chen[b,*] and Xile Hu[a*]

[a] Laboratory of Inorganic Synthesis and Catalysis, Institute of Chemical Sciences and Engineering, Ecole Polytechnique Fédérale de Lausanne (EPFL)

Lausanne CH-1015, Switzerland

[b] Department of Chemistry, National Taiwan University, Taipei, Taiwan

*Corresponding author: Email: haomingchen@ntu.edu.tw; xile.hu@epfl.ch;

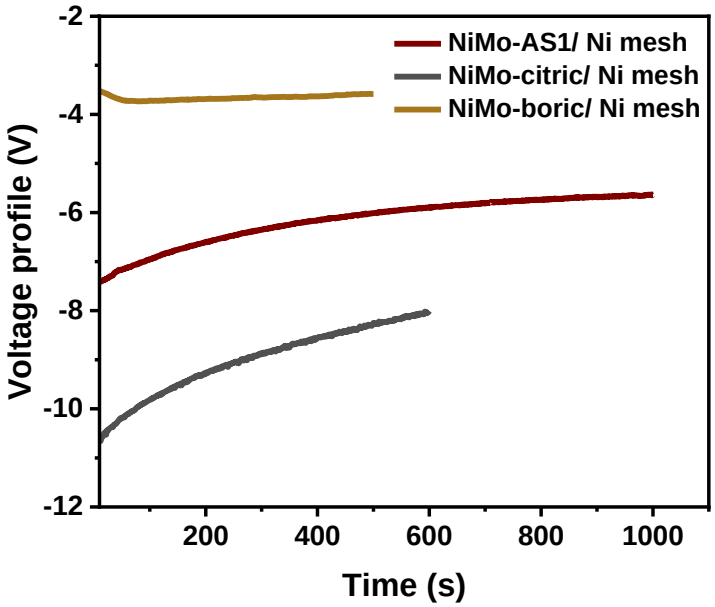

Fig.S1. Voltage profile during the electrodeposition of the NiMo catalysts on Ni mesh.

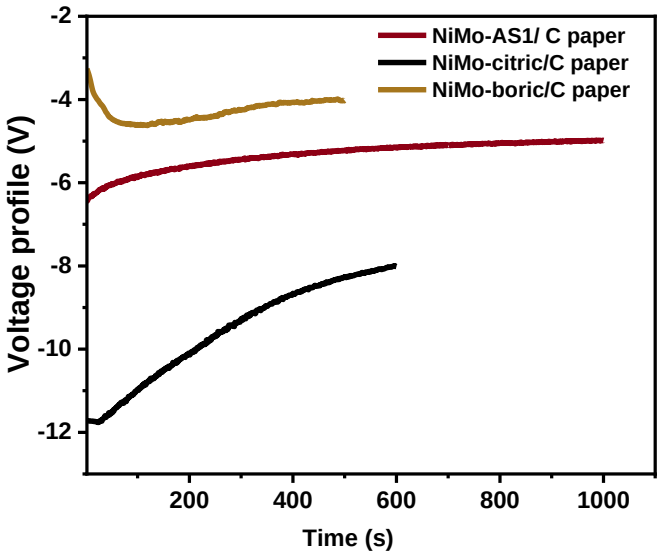

Fig.S2. Voltage profile during the electrodeposition of the NiMo catalysts on C paper support

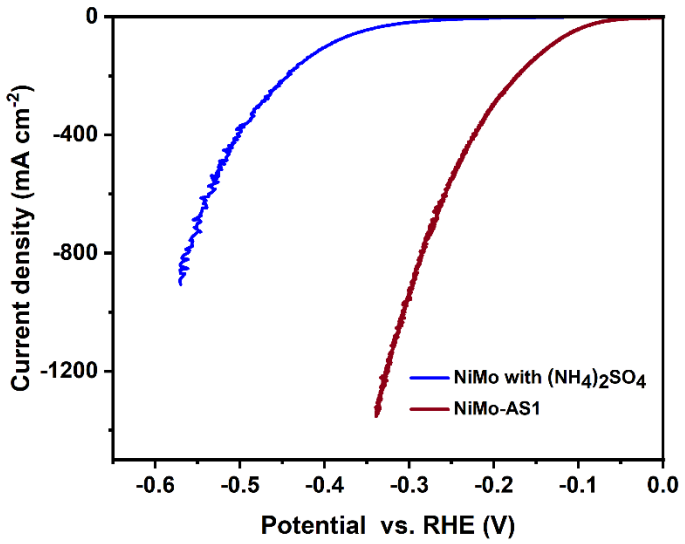

Fig.S3. Comparison of LSV curves of NiMo-AS1 catalyst with a similarly made catalyst where NH_4Cl in the deposition bath was replaced by $(NH_4)_2SO_4$.

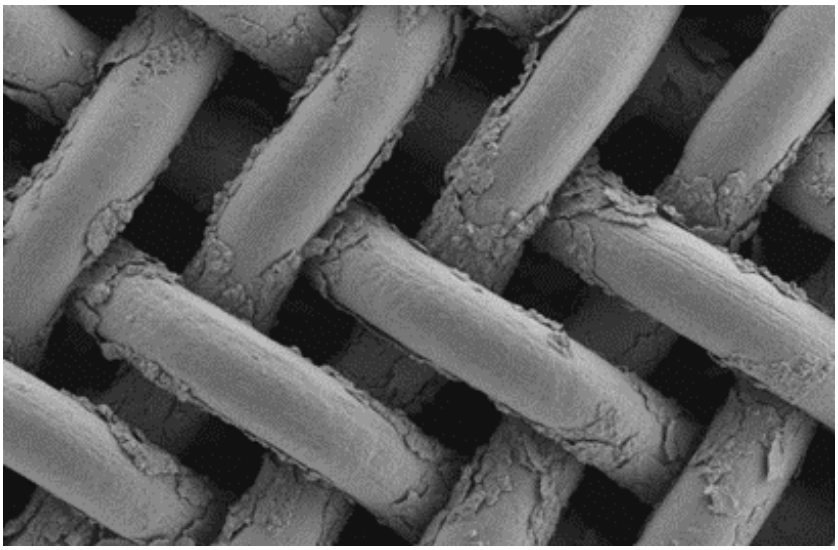

Fig.S4. SEM image of the NiMo catalyst made with $(NH_4)_2SO_4$ (see Fig. S3) after one LSV measurement

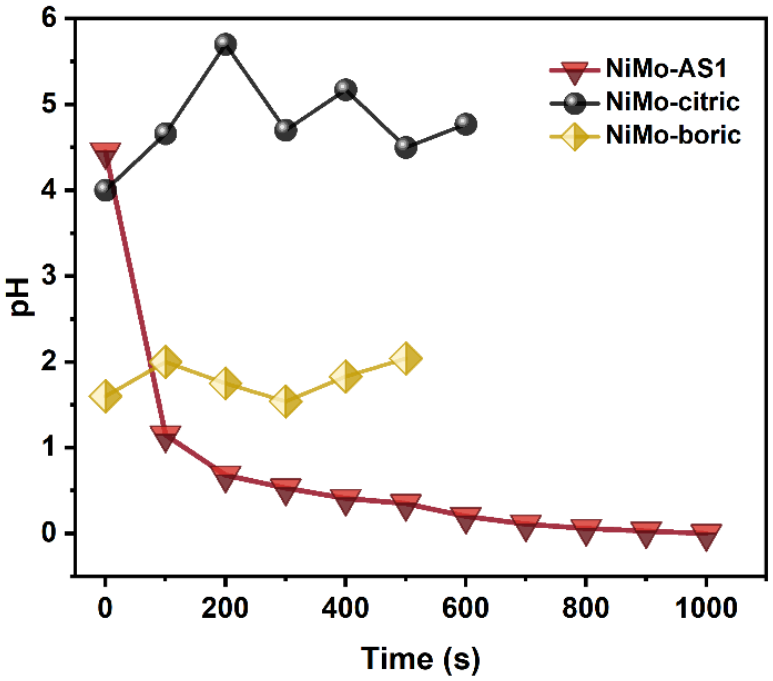

Fig.S5. pH profile during the electrodeposition of NiMo catalysts.

A

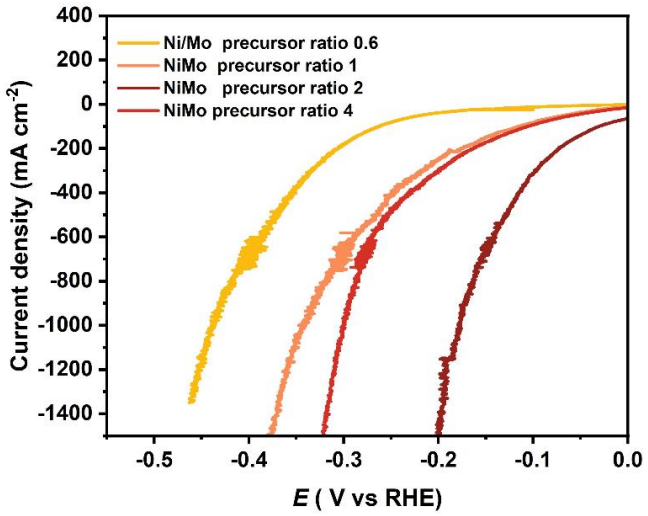
Ni/Mo precursor ratio 0.6
NiMo precursor ratio 1
NiMo precursor ratio 2
NiMo precursor ratio 4
Current density (mA cm-2)
E (V vs RHE)
400
200
0
-200
-400
-600
-800
-1000
-1200
-1400
-0.5
-0.4
-0.3
-0.2
-0.1
0.0

B

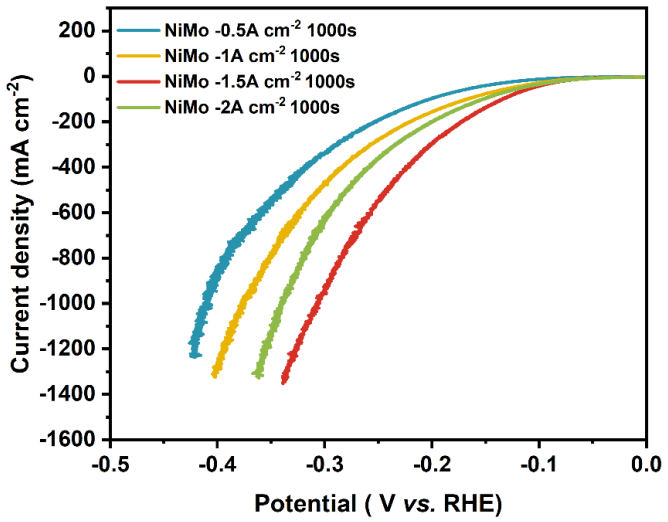
NiMo -0.5A cm-2 1000s
NiMo -1A cm-2 1000s
NiMo -1.5A cm-2 1000s
NiMo -2A cm-2 1000s
Current density (mA cm-2)
Potential (V vs. RHE)
200
0
-200
-400
-600
-800
-1000
-1200
-1400
-1600
-0.5
-0.4
-0.3
-0.2
-0.1
0.0

C

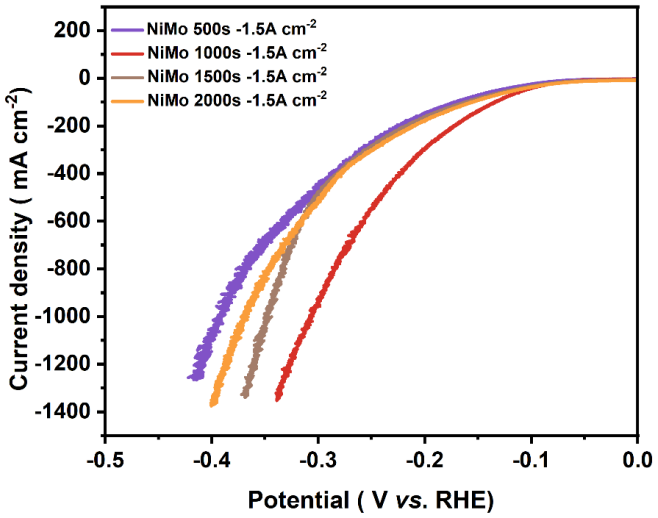

Fig.S6. A. LSVs of NiMo catalysts made using different Ni/Mo precursor ratios; B. LSVs of NiMo catalysts made using different electrodeposition currents; C. LSVs of NiMo catalysts made using different electrodeposition times.

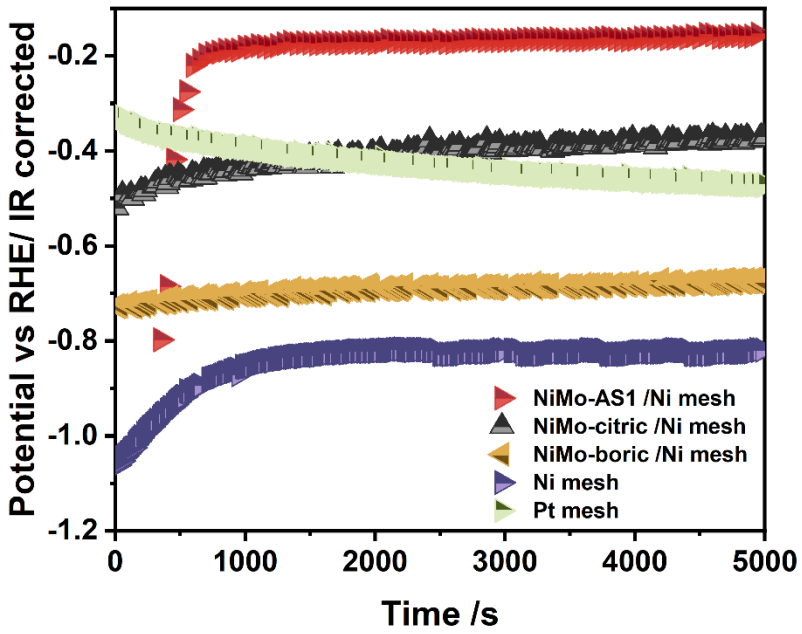

Fig.S7. Activation process at 1 A cm^{-2} for the NiMo catalysts on Ni mesh, bare Ni mesh, and Pt mesh.

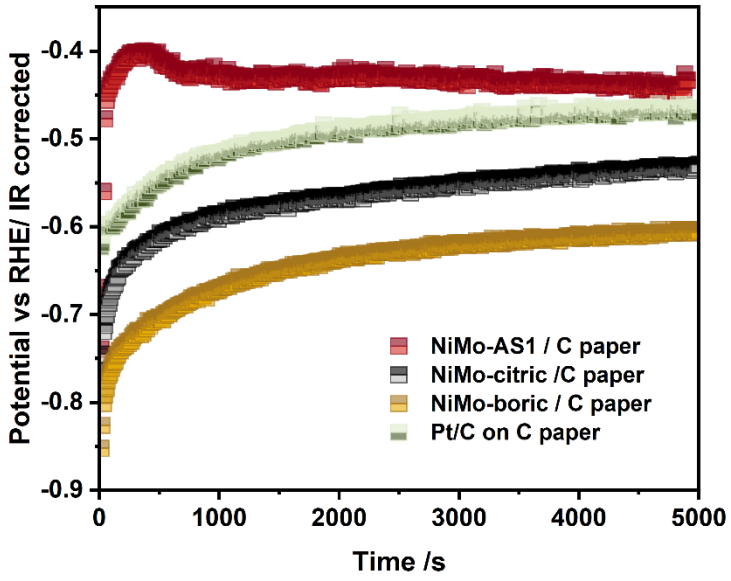

Fig.S8. Activation process at 1 A cm^{-2} for the NiMo catalysts and Pt/C on C paper .

A

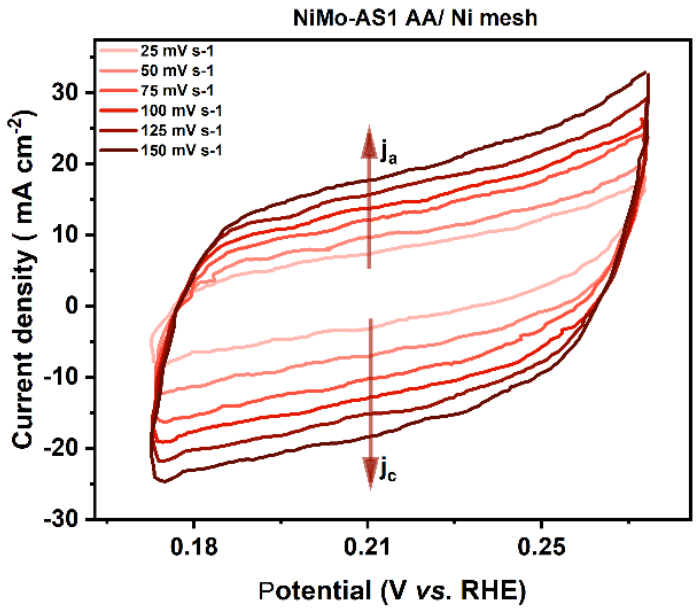
NiMo-AS1 AA/ Ni mesh
25 mV s-1
50 mV s-1
75 mV s-1
100 mV s-1
125 mV s-1
150 mV s-1
j_a
j_c
Current density (mA cm^{-2})
30
20
10
0
-10
-20
-30
0.18
0.21
0.25
Potential (V *vs.* RHE)

B

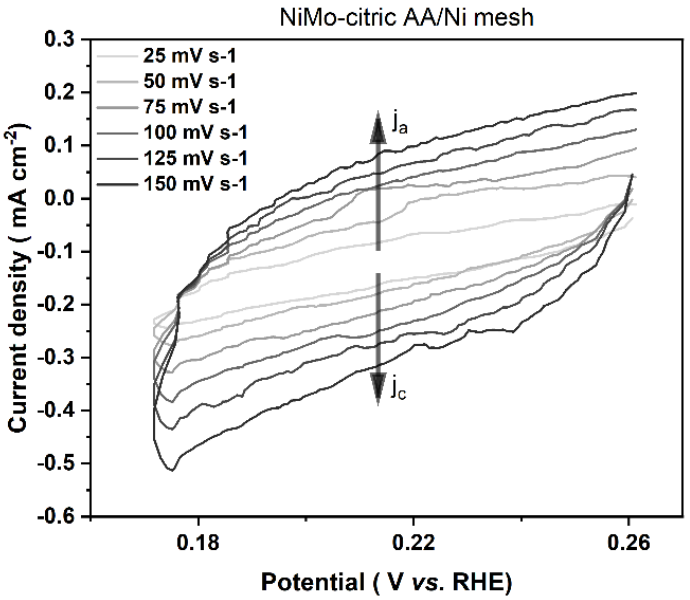
NiMo-citric AA/Ni mesh
25 mV s-1
50 mV s-1
75 mV s-1
100 mV s-1
125 mV s-1
150 mV s-1
j_a
j_c
Current density (mA cm^{-2})
0.3
0.2
0.1
0.0
-0.1
-0.2
-0.3
-0.4
-0.5
-0.6
0.18
0.22
0.26
Potential (V *vs.* RHE)

C

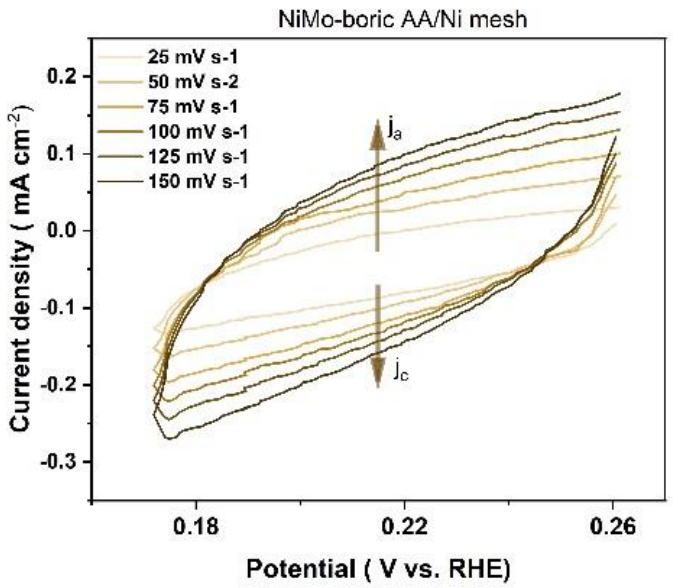
NiMo-boric AA/Ni mesh
25 mV s-1
50 mV s-2
75 mV s-1
100 mV s-1
125 mV s-1
150 mV s-1
j_a
j_c
Current density (mA cm^{-2})
0.2
0.1
0.0
-0.1
-0.2
-0.3
0.18
0.22
0.26
Potential (V vs. RHE)

D

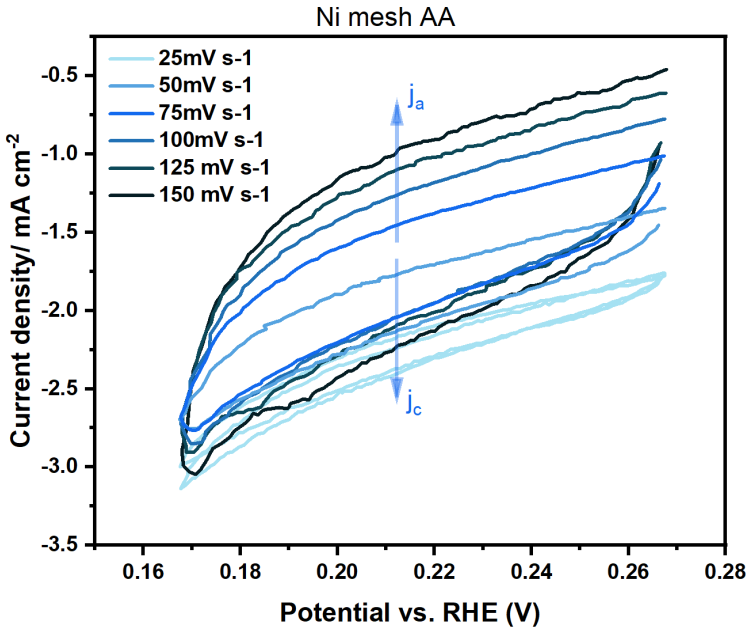
Ni mesh AA
25mV s-1
50mV s-1
75mV s-1
100mV s-1
125 mV s-1
150 mV s-1
j_a
j_c
Current density/ mA cm^{-2}
-0.5
-1.0
-1.5
-2.0
-2.5
-3.0
-3.5
0.16
0.18
0.20
0.22
0.24
0.26
0.28
Potential vs. RHE (V)

E

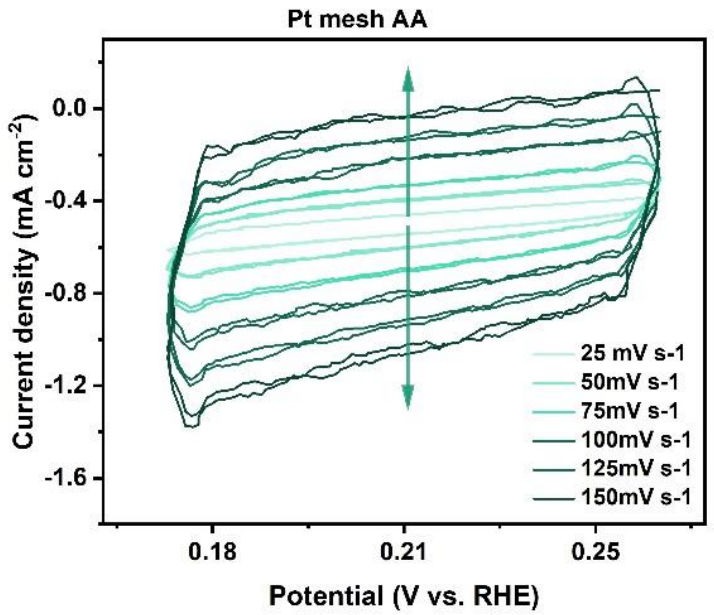

Fig.S9. CVs in the non-faradaic region after the activation process (AA) of the NiMo catalysts on Ni mesh, bare Ni, and Pt mesh.

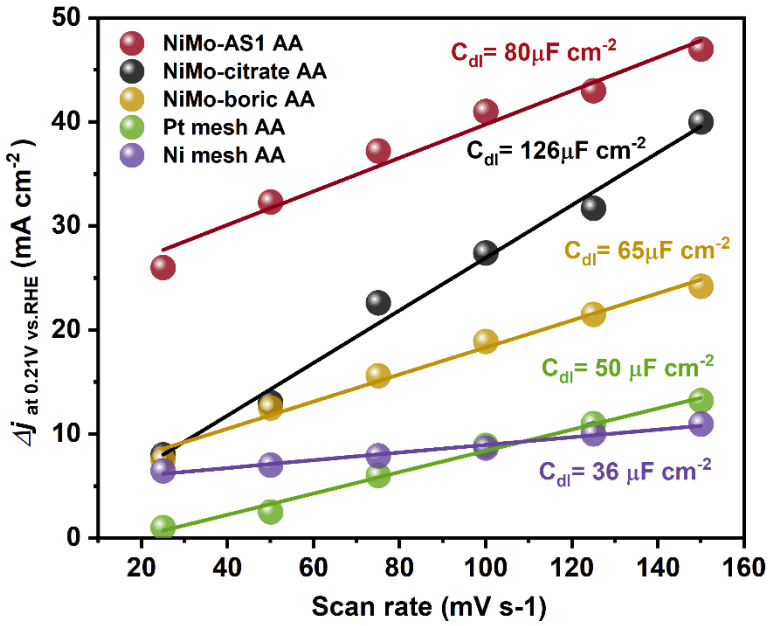

Fig.10. The double-layer capacitances of the activated (AA) NiMo catalysts on Ni mesh, barre Ni and Pt mesh.

A

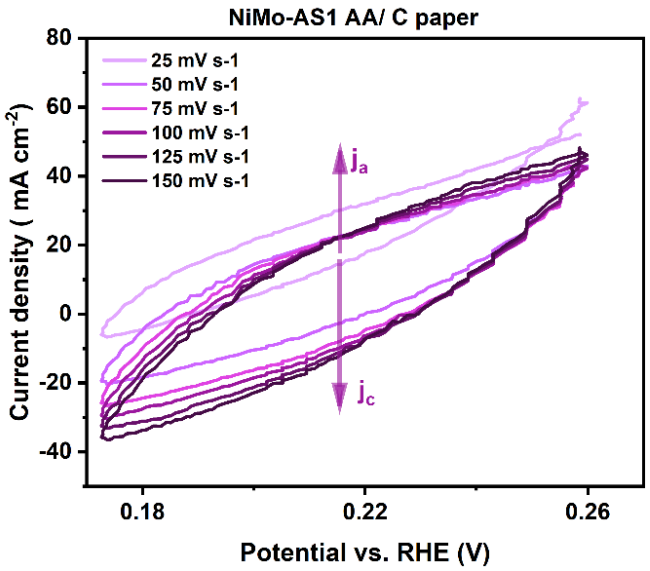
NiMo-AS1 AA/ C paper
25 mV s-1
50 mV s-1
75 mV s-1
100 mV s-1
125 mV s-1
150 mV s-1
j_a
j_c
Current density (mA cm^{-2})
Potential vs. RHE (V)
80
60
40
20
0
-20
-40
0.18
0.22
0.26

B

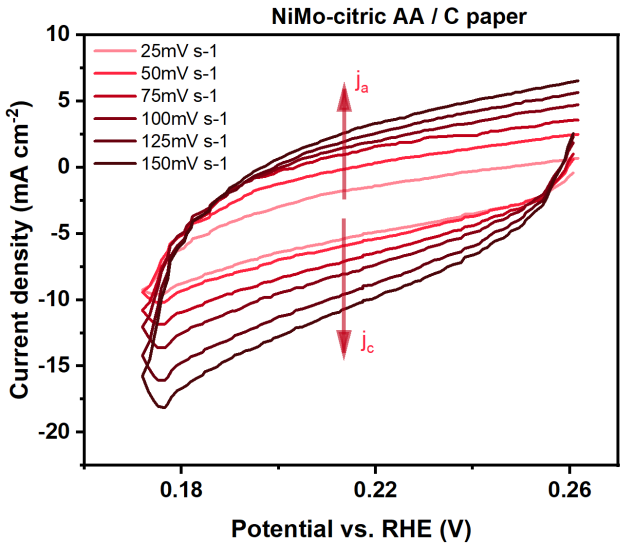
NiMo-citric AA / C paper
25mV s-1
50mV s-1
75mV s-1
100mV s-1
125mV s-1
150mV s-1
j_a
j_c
Current density (mA cm^{-2})
Potential vs. RHE (V)
10
5
0
-5
-10
-15
-20
0.18
0.22
0.26

C

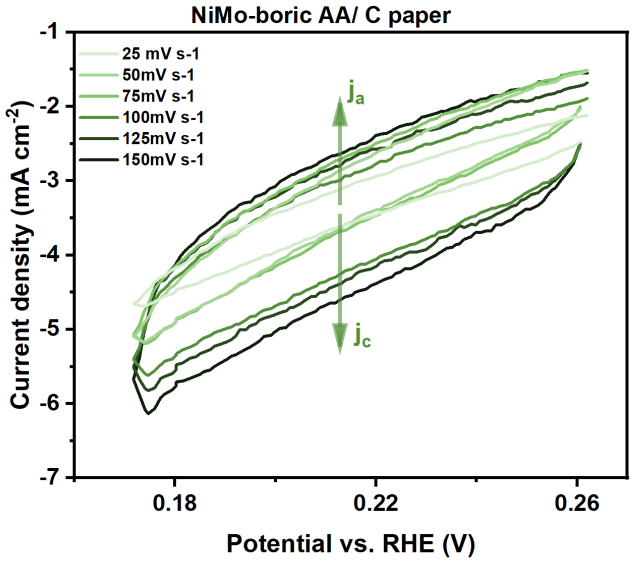
NiMo-boric AA/ C paper
25 mV s-1
50mV s-1
75mV s-1
100mV s-1
125mV s-1
150mV s-1
j_a
j_c
Current density (mA cm^{-2})
-1
-2
-3
-4
-5
-6
-7
0.18
0.22
0.26
Potential vs. RHE (V)

D

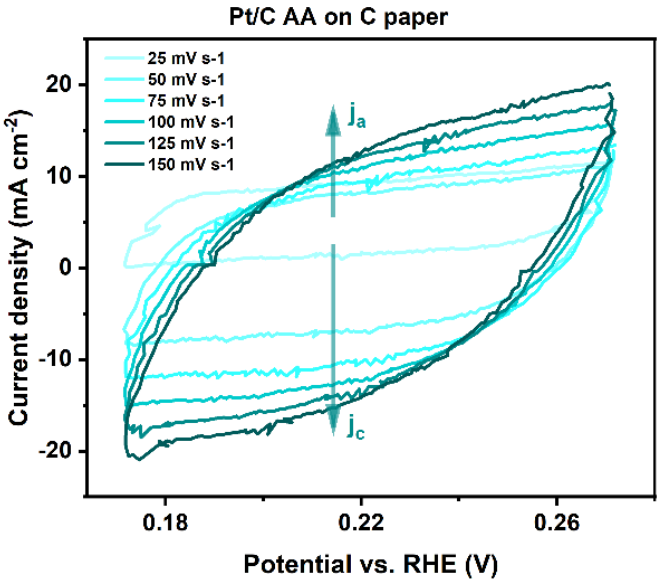
Pt/C AA on C paper
25 mV s-1
50 mV s-1
75 mV s-1
100 mV s-1
125 mV s-1
150 mV s-1
j_a
j_c
Current density (mA cm^{-2})
20
10
0
-10
-20
0.18
0.22
0.26
Potential vs. RHE (V)

E

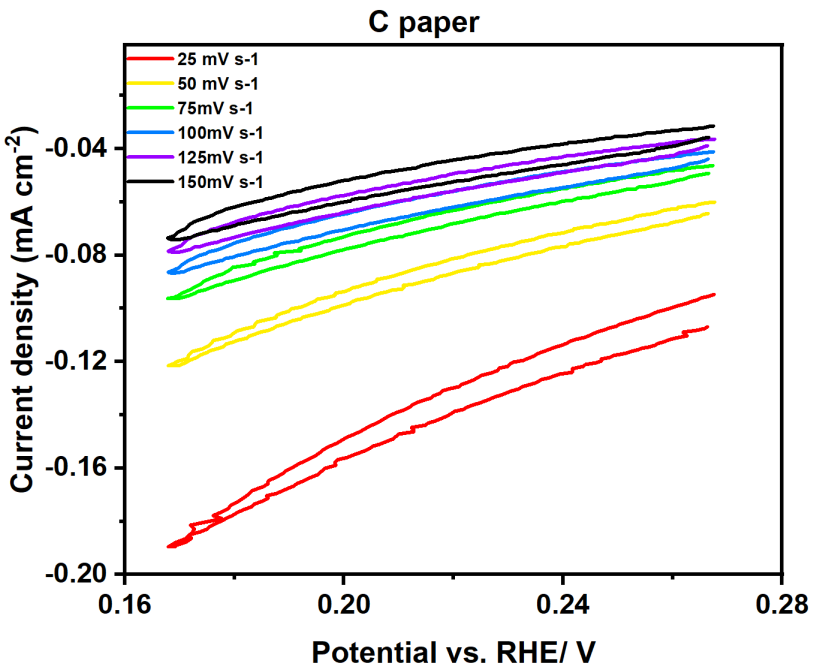

Fig.S11. CVs in the non-faradaic region after the activation process (AA) of the NiMo catalysts on C, Pt/C on C, and bare C paper. The capacitive current densities for bare carbon paper are negligible compared to those of the other samples.

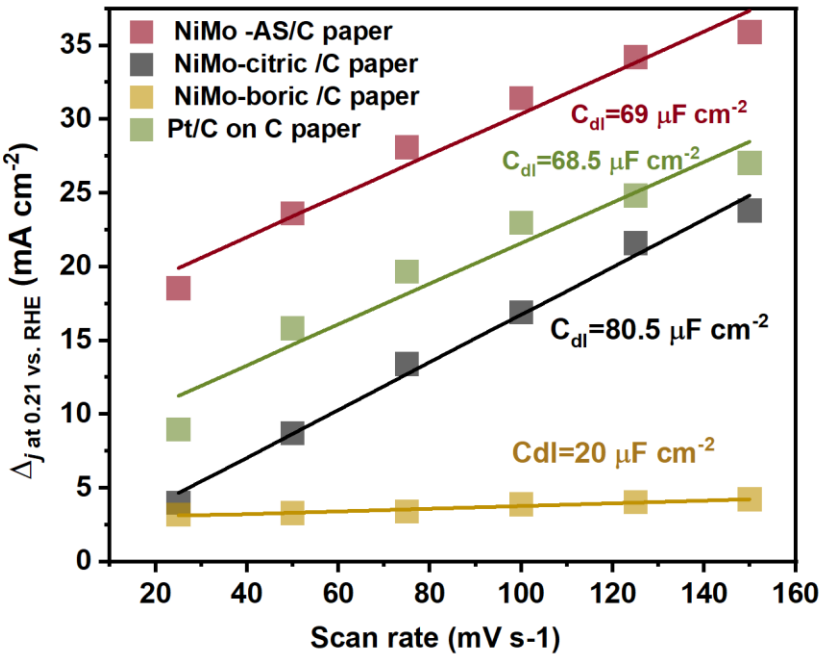

Fig.S12. The double-layer capacitances of the activated (AA) NiMo catalysts on C, Ni mesh, Pt/C on C, and bare C paper.

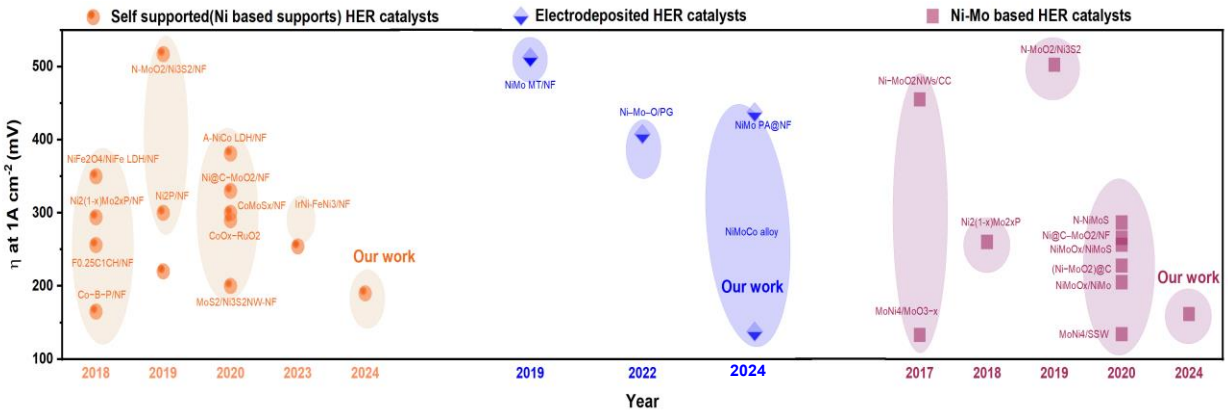

Fig.S13 Comparison of the overpotential at 1 A cm^{-2} with other reported catalysts.[1-19]

The comparison was made based on their activity in a conventional 3-electrode setup.

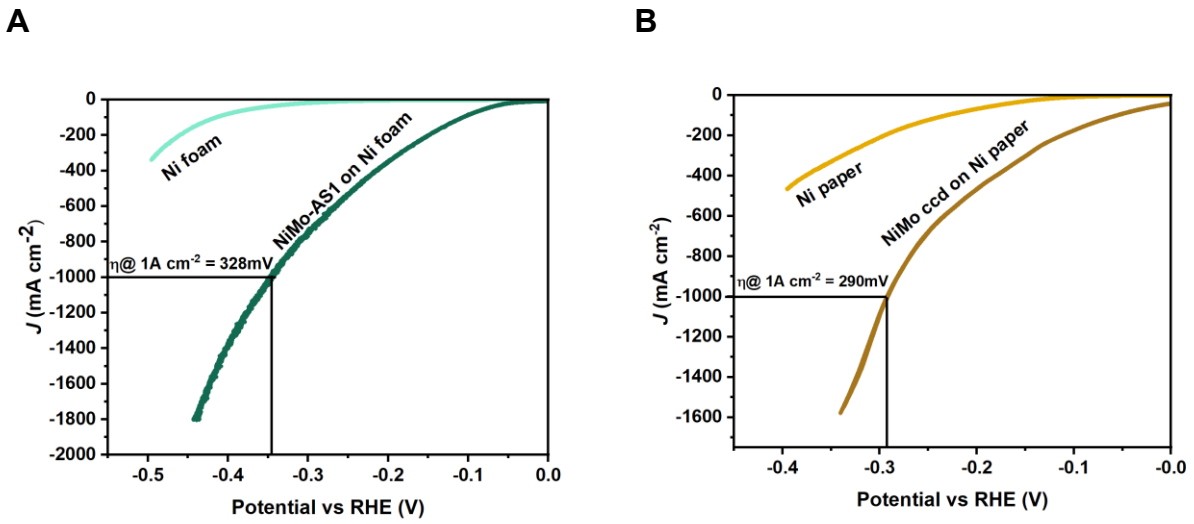

Fig.S14. A: LSV of bare Ni foam and NiMo-AS1 deposited on Ni foam. B: LSV of bare Ni paper and NiMo-AS1 deposited on Ni paper.

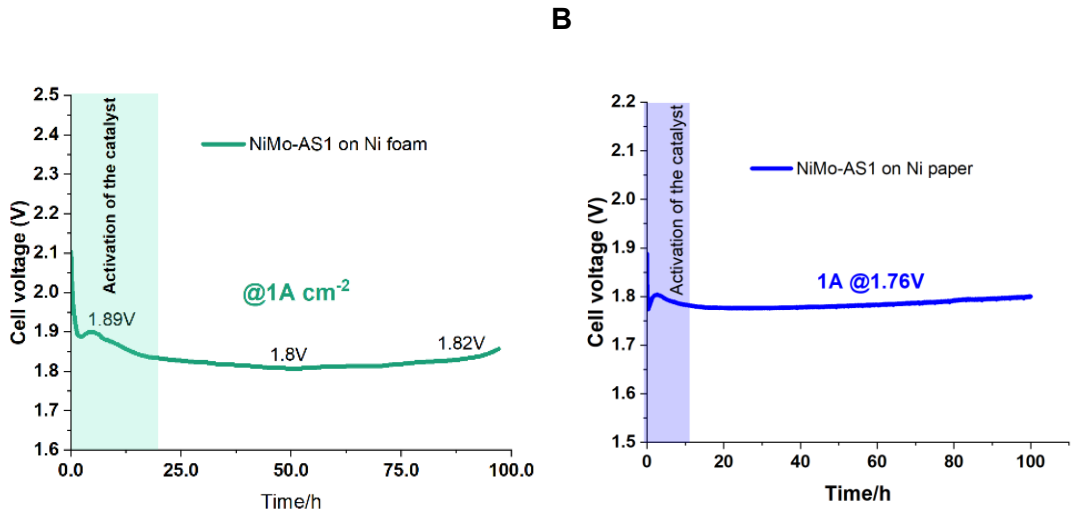

Fig.S15. Long-term electrolysis data at a constant current density of 1 A/cm^2 and cell temperature of 80°C of (A) NiMo-AS1 on Ni foam and (B)NiMo-AS1 on Ni paper

TOP:

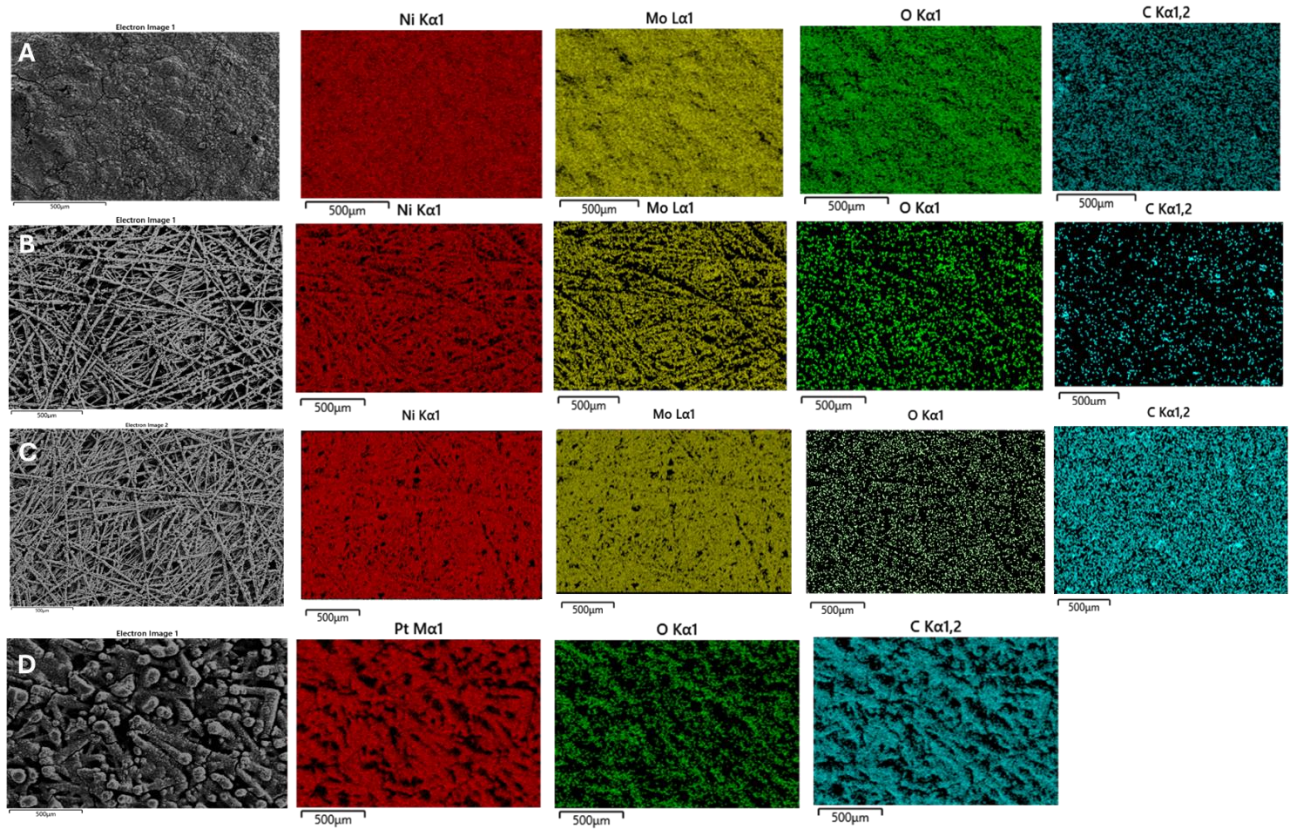
A
B
C
D
Electron Image 1
Electron Image 2
Ni Kα1
Mo Lα1
O Kα1
C Kα1,2
Pt Mα1
500µm

Bottom:

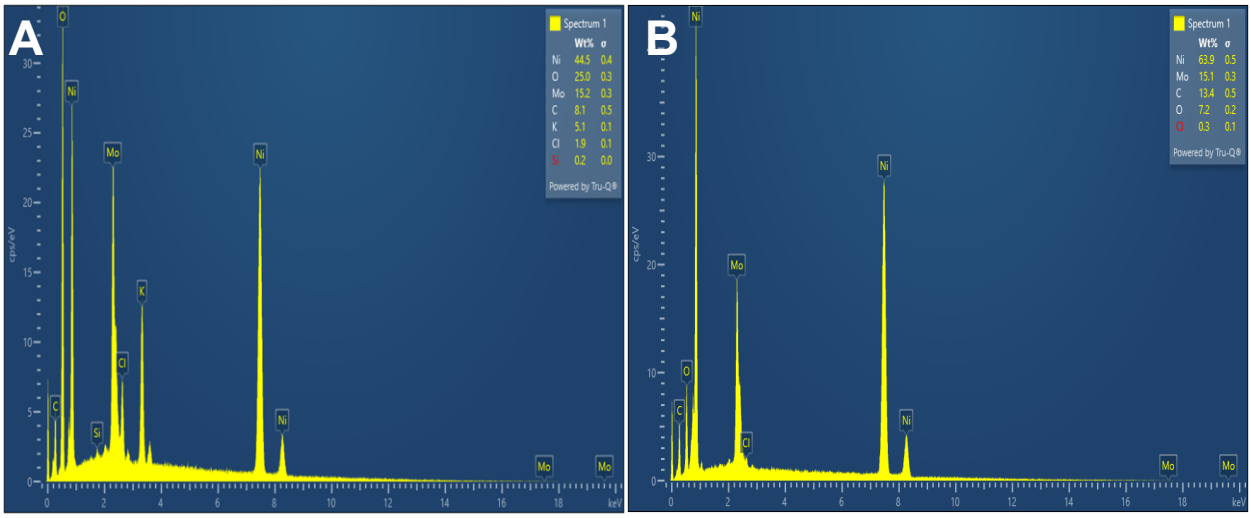
A
B
Spectrum 1
Wt% σ
Ni 44.5 0.4
O 25.0 0.3
Mo 15.2 0.3
C 8.1 0.5
K 5.1 0.1
Cl 1.9 0.1
Si 0.2 0.0
Powered by Tru-Q®
Spectrum 1
Wt% σ
Ni 63.9 0.5
Mo 15.1 0.3
C 13.4 0.5
O 7.2 0.2
Cl 0.3 0.1
Powered by Tru-Q®
cps/eV
keV

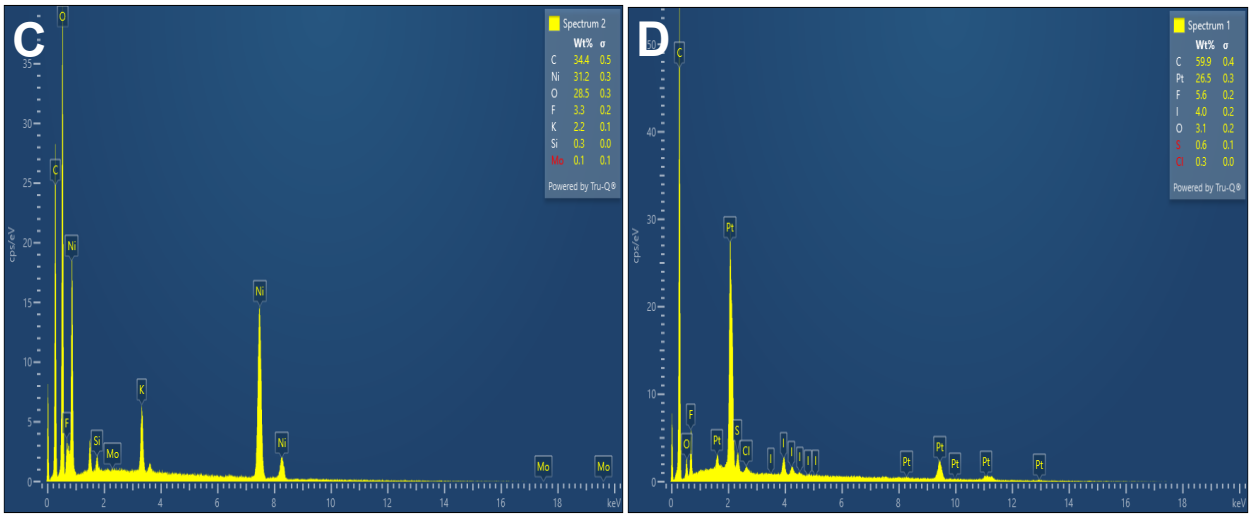

Fig. S16. (Top) SEM images and EDX mapping of the as-prepared catalysts on C paper. (Bottom) Element mapping showing the weight percentages for different samples. A: NiMo-AS1; B: NiMo-citric; C: NiMo-boric; D: Pt/C.

Top

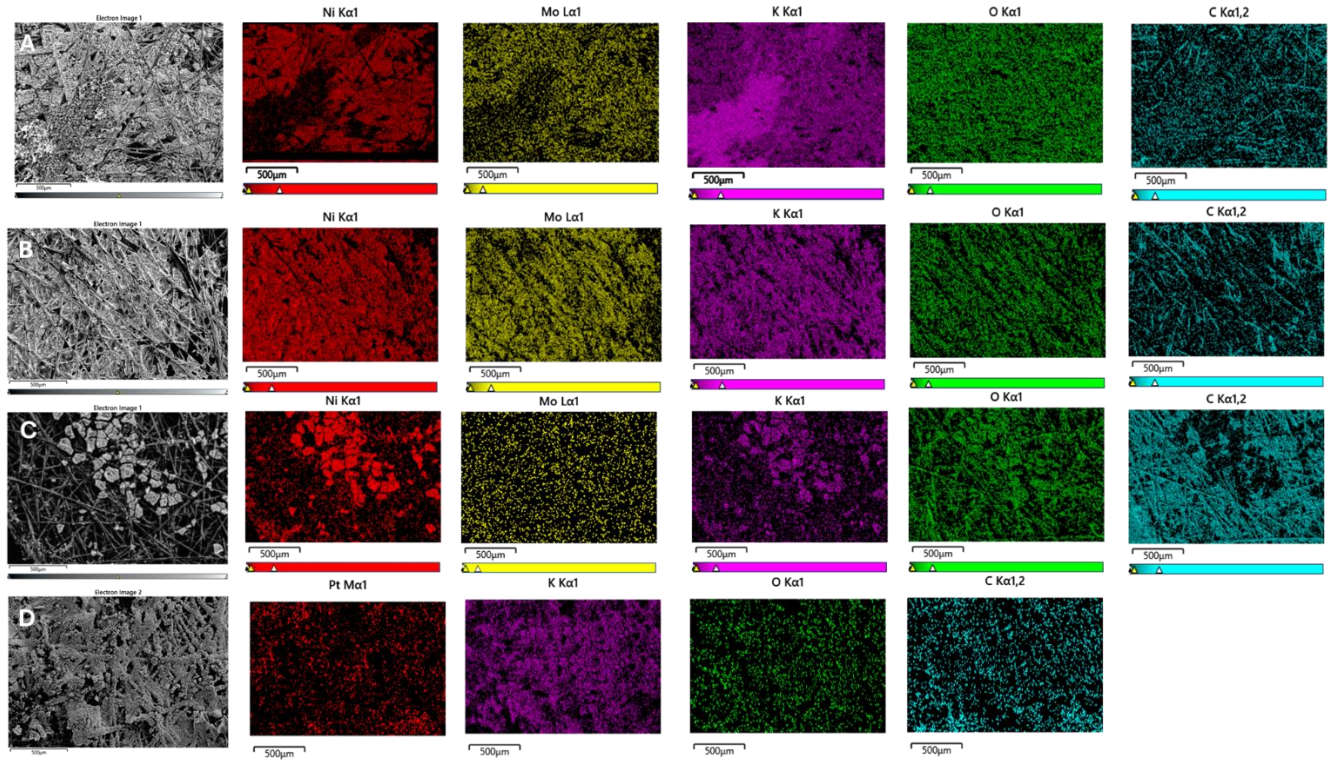
A
B
C
D
Ni Kα1
Mo Lα1
K Kα1
O Kα1
C Kα1,2
Pt Mα1
500µm

Bottom.

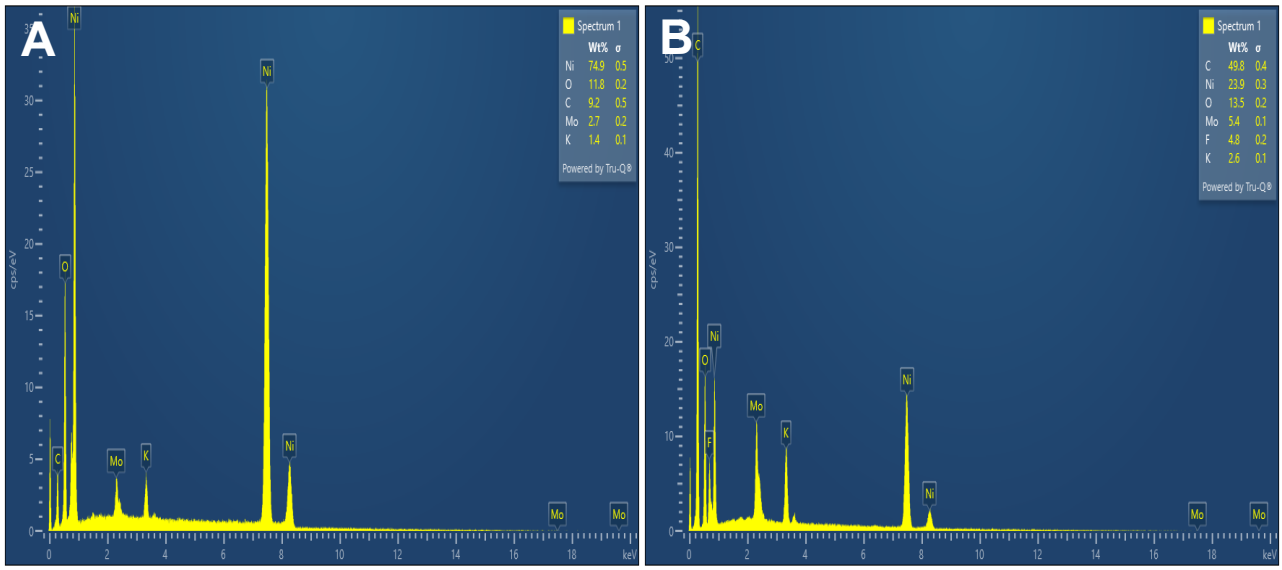
A
Spectrum 1
Wt% σ
Ni 74.9 0.5
O 11.8 0.2
C 9.2 0.5
Mo 2.7 0.2
K 1.4 0.1
Powered by Tru-Q®
B
Spectrum 1
Wt% σ
C 49.8 0.4
Ni 23.9 0.3
O 13.5 0.2
Mo 5.4 0.1
F 4.8 0.2
K 2.6 0.1
Powered by Tru-Q®
cps/eV
keV

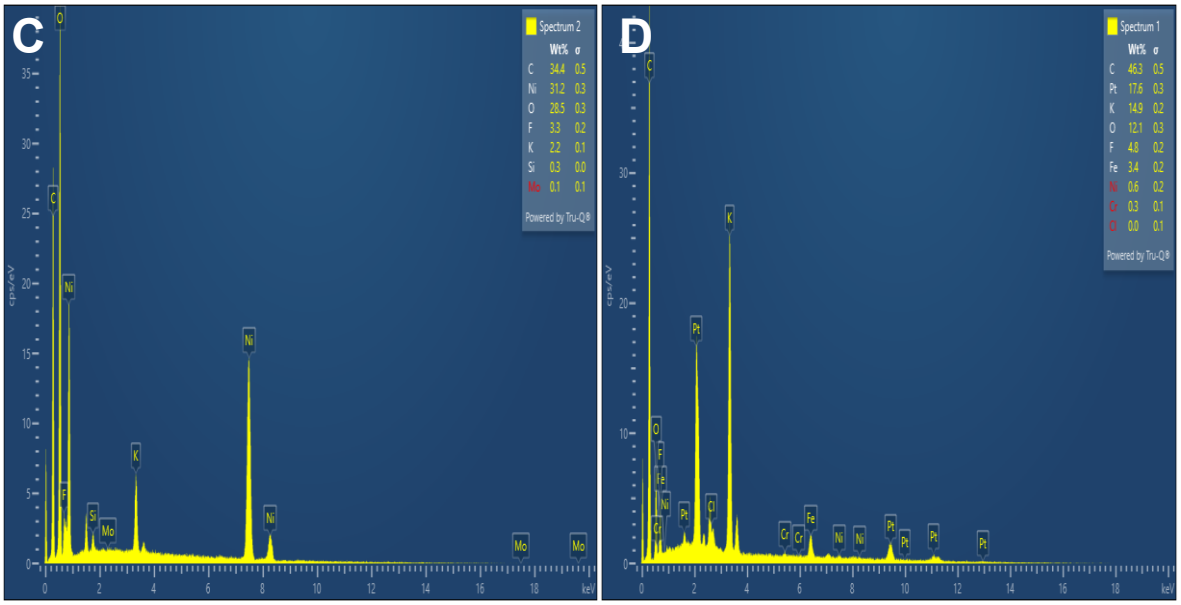

Fig. S17. (Top) SEM images and EDX mapping of the catalysts on C paper after operating at 3 A cm-2 for 150 h. (Bottom) Element mapping showing the weight percentages for different samples. A: NiMo-AS1; B: NiMo-citric; C: NiMo-boric; D: Pt/C.

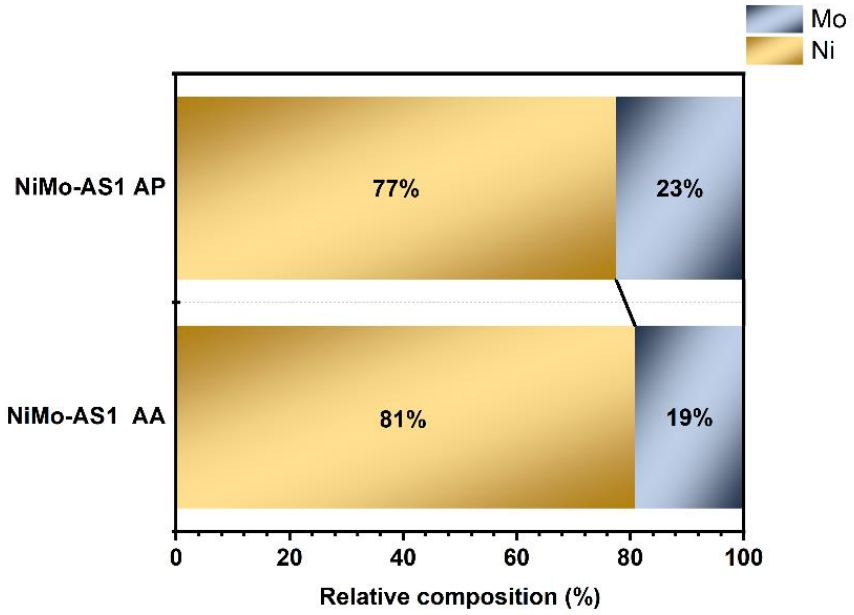

Fig.S18. ICP-MS result of the NiMo-AS1 catalyst in the as-prepared state (AP) and after activation (AA) at 1 A cm^{-2} for 2 h; relative composition is referring to mol ratio.

We describe the averaged ICP-MS results, with the Standard error and deviation in Tabel S4.

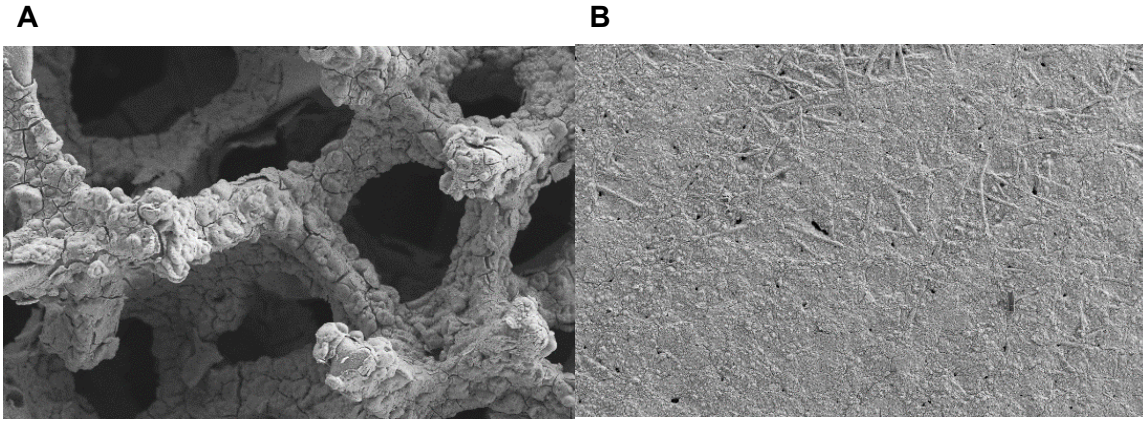

Fig.S19. SEM images of the initial NiMo-AS1 on (A) Ni foam and (B) Ni paper.

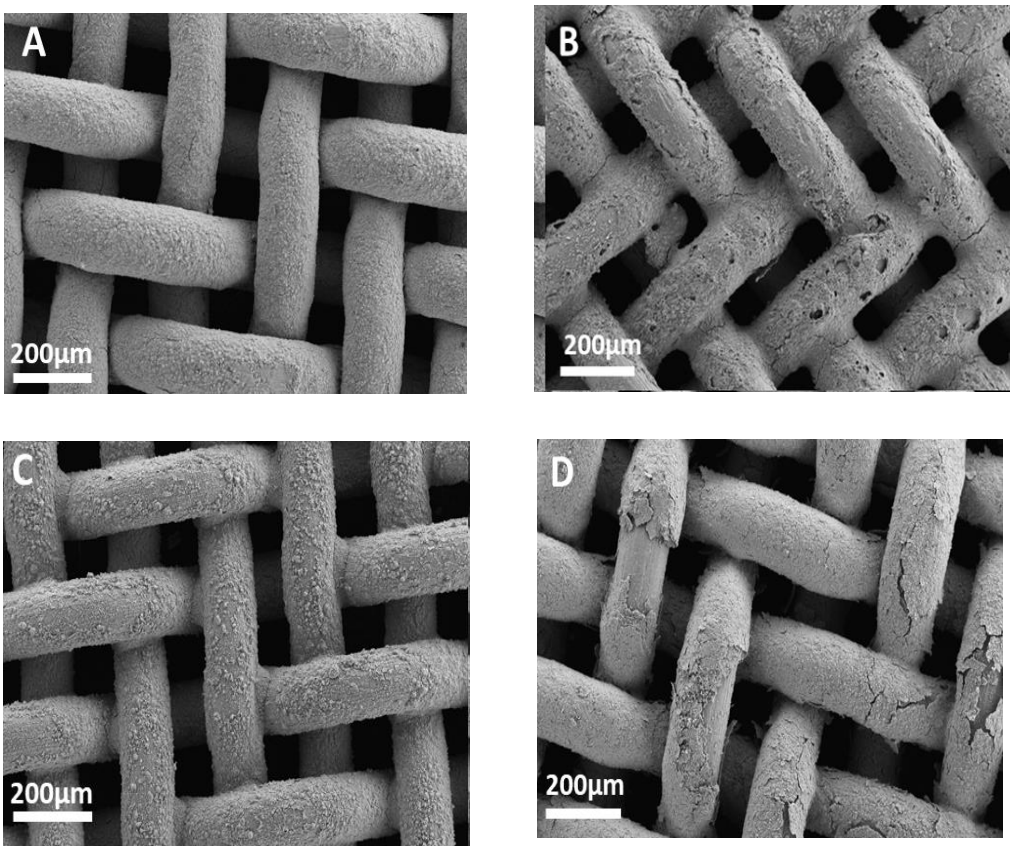

Fig.S20. SEM images of: (A) NiMo-AS electrodeposited at -0.5 A/cm^2; (B) NiMo-AS electrodeposited at -1 A/cm^2; (C) NiMo-AS electrodeposited at -1.5 A/cm^2; (D) NiMo-AS electrodeposited at -2 A/cm^2 for 1000 s.

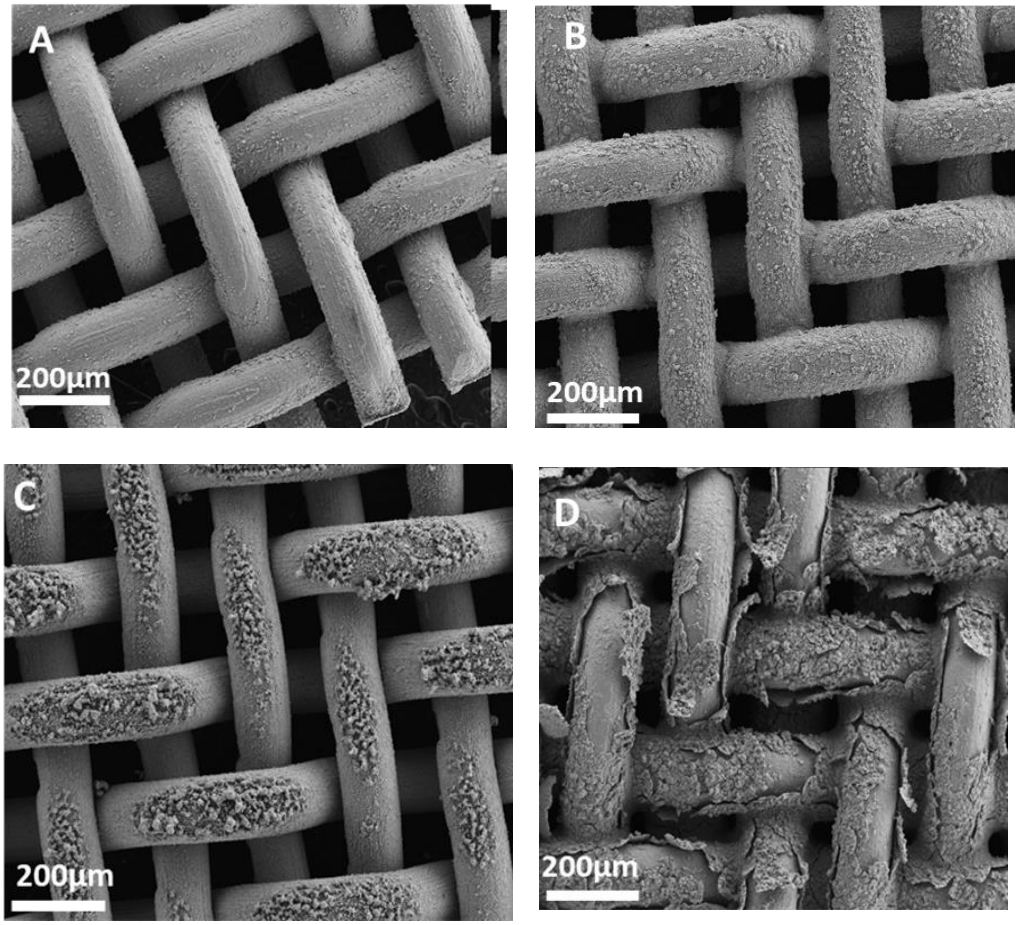

Fig.S21. SEM images of NiMo-As electrodeposited at -1.5 A/cm^2 for: (A) 500 s; (B) 1000 s; (C) 1500 s; (D) 2000 s.

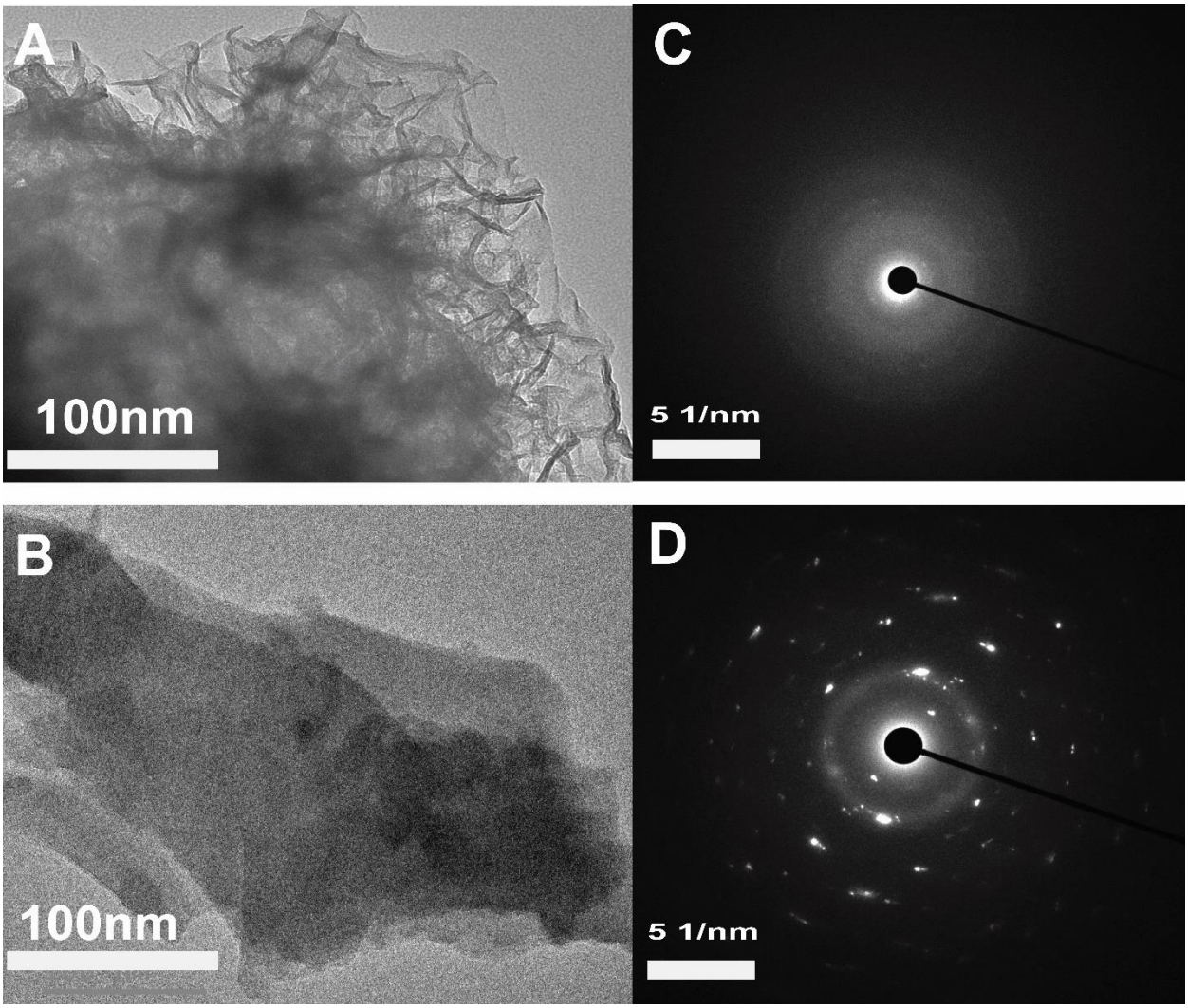

Fig. S22. (A) TEM image of the as-prepared NiMo-AS1; (B) SAED pattern of the as-prepared NiMo-AS1; (C) TEM image of theNiMo-AS1 after HER at 1 A/cm^2; (D) SAED pattern of the NiMo-AS1 after HER at 1 A/cm^2.

The protocol for catalyst detachment from the Ni mesh substrate consisted of immersing the as prepared NiMo -AS1 on Ni mesh and after the HER at -1 A cm^{-2} for 30 min in 10 mL deionized (DI) water in an ultrasonication bath for 30 min. Afterwards, the DI was evaporated by keeping the solution in a drying oven at 120°C. The powder was collected and dispersed in 2 mL isopropanol. The solution was ultrasonicated and dispersed on the TEM grit by using a micropipette.

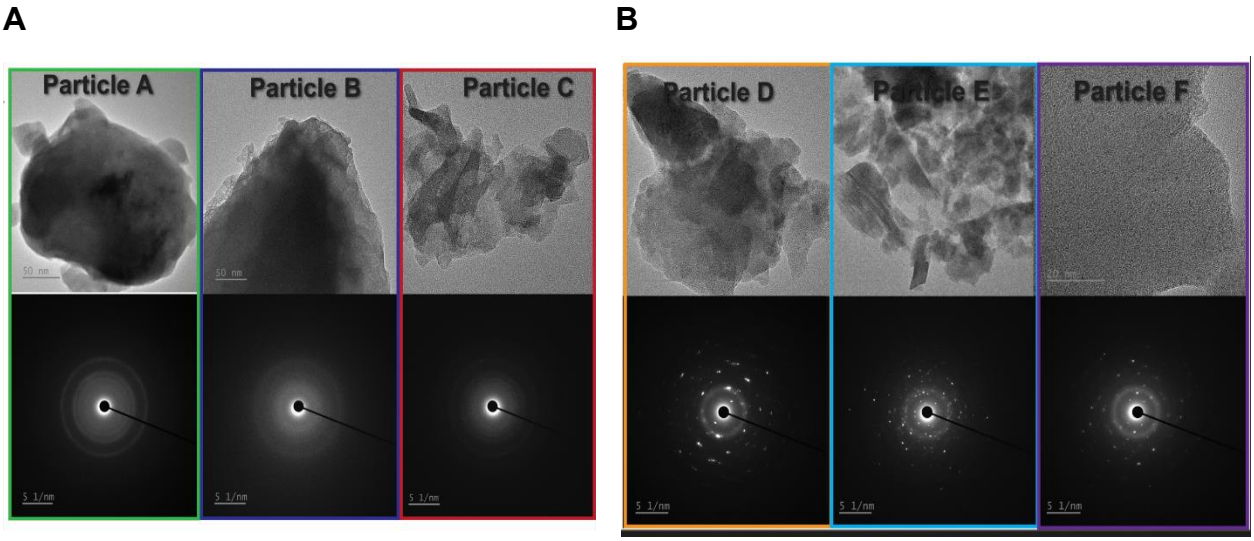

Fig.S23. (A) TEM and SAED profiles of different particles for the as-prepared NiMo -AS1 catalyst (B) TEM and SAED profiles of different particles for the NiMo -AS1 catalyst after HER at -1 A cm^{-2}

Transmission Electron Microscopy (TEM) was employed to examine different particles of the NiMo-AS1 catalyst, both in its as-prepared state and after undergoing the Hydrogen Evolution Reaction (HER) at -1 A cm^{-2}. The Selected Area Electron Diffraction (SAED) profiles were averaged in both cases to ensure a more precise interpretation of the results.

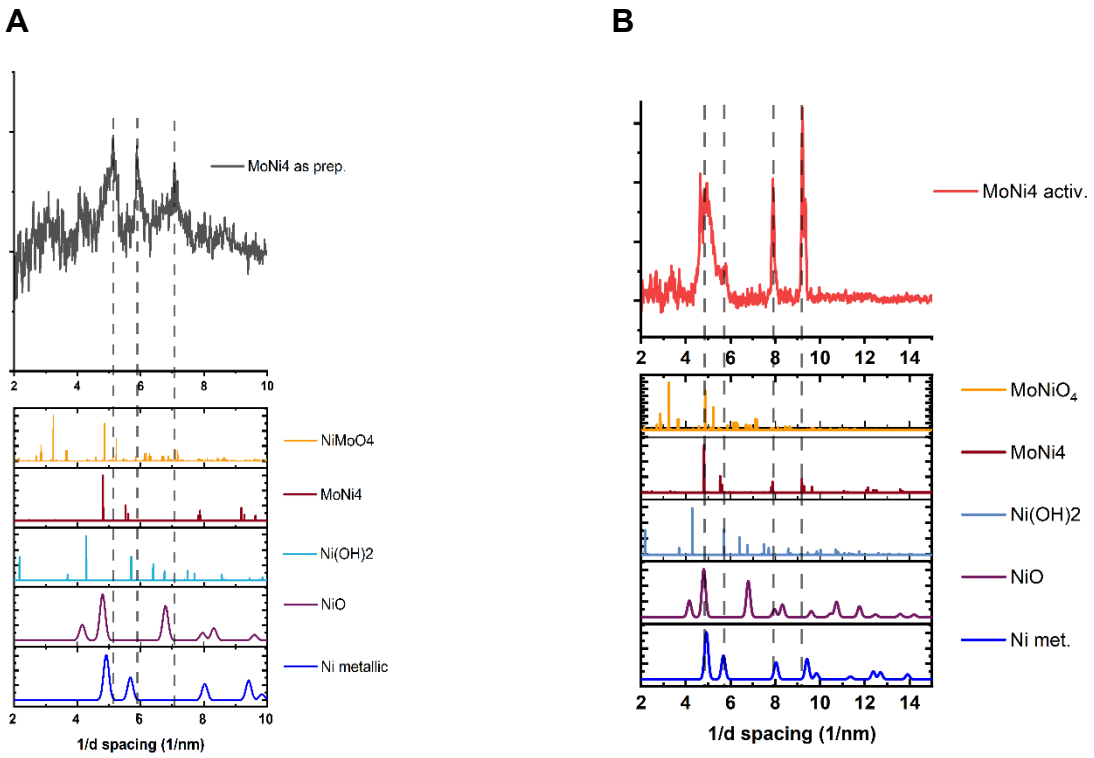

Fig.S24 (A) SAED d values and simulated patterns for the as-prepared NiMo -AS1 (B) SAED d values and simulated patterns for NiMo -AS1 after high current density HER.

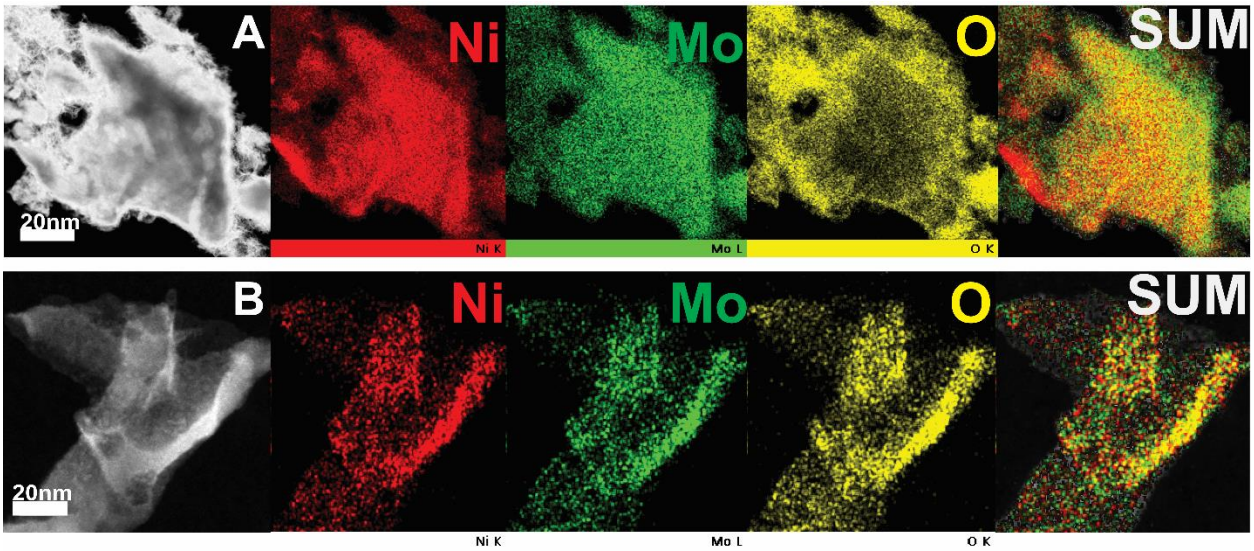

Fig.S25. EDX mapping of NiMo-AS1: (A) in the as prepared state; (B) after after HER at 1A/cm^2.

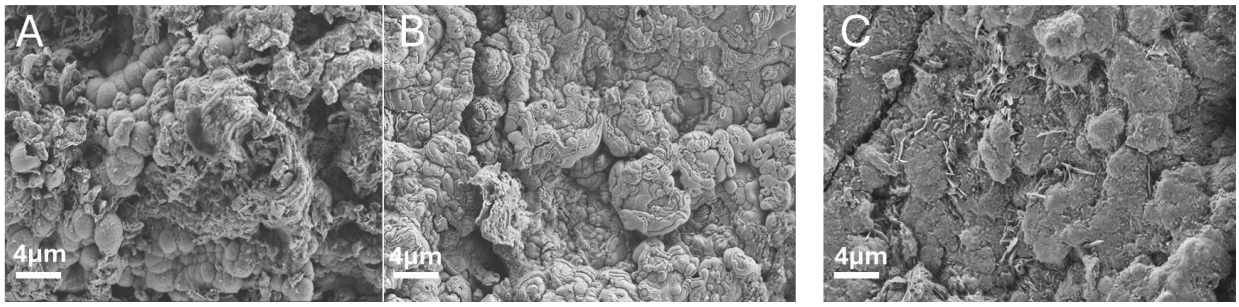

Fig.S26. SEM images of NiMo-AS1 after 100 h of electrolysis at 1A/cm^2 at different temperatures. A: 24◦C; B: 40◦C ; C: 80◦C.

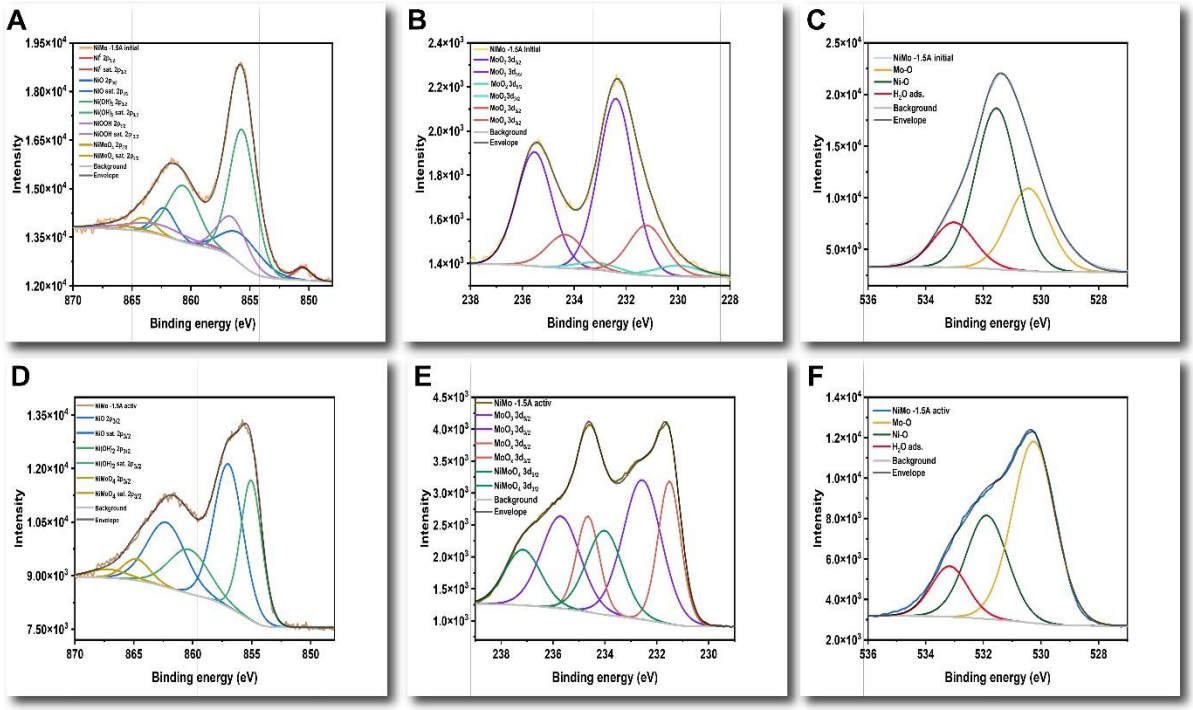

Fig.S27. The XPS spectra of as-prepared NiMo -AS1 (A-C) (A) Ni $2p_{3/2}$ (B) Mo $3d_{3/2\text{-}5/2}$ (C) O 1s. And XPS spectra of NiMo -AS1 after HER at -1 A cm^{-2} (D-E) (D) Ni $2p_{3/2}$ (E) Mo $3d_{3/2\text{-}5/2}$ (F) O 1s.

The intensity of the molybdenum species has nearly doubled post ER at a high current density. This result suggests that during the reaction, Mo species migrated from a deeper layer within the catalyst to the surface layer.

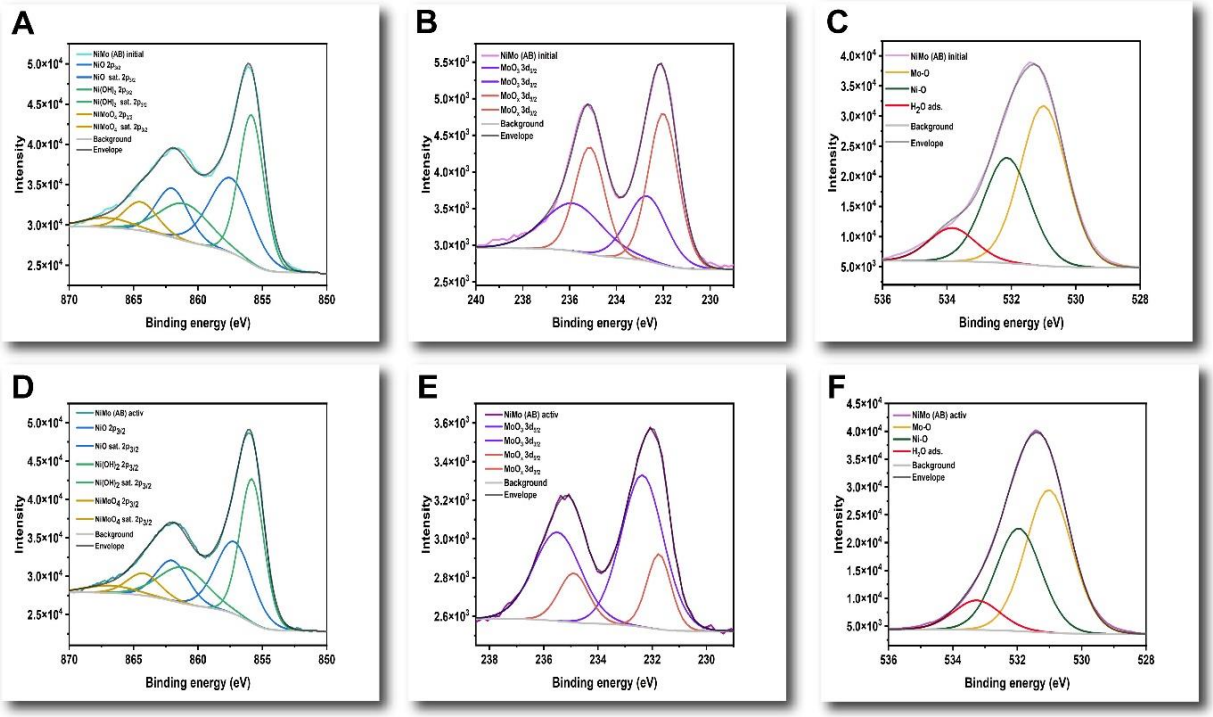

Fig.S28. The XPS spectra of as-prepared NiMo-citric (A-C) (A) Ni $2p_{3/2}$ (B) Mo $3d_{3/2\text{-}5/2}$ (C) O 1s. And XPS spectra of NiMo-citric after HER at -1 A cm^{-2} (D-E) (D) Ni $2p_{3/2}$ (E) Mo $3d_{3/2\text{-}5/2}$ (F) O 1s.

In the case of the NiMo-citric sample, a reduction in Mo spectra intensity is observed after HER.

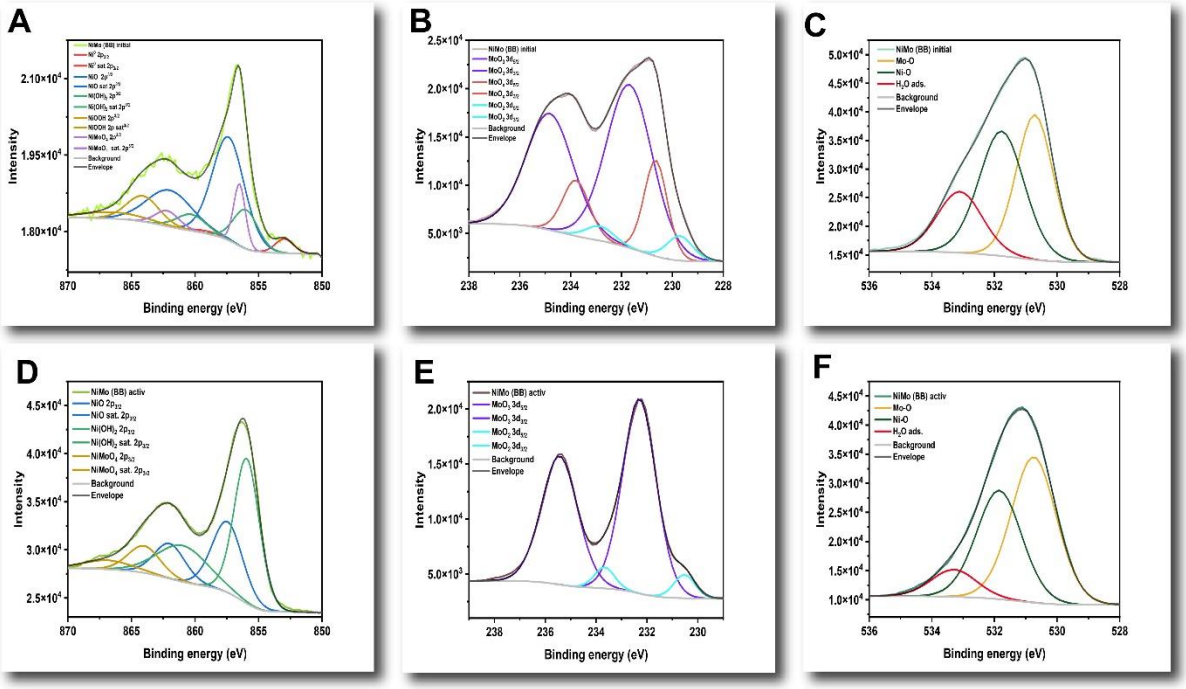

Fig.S29. The XPS spectra of the as-prepared NiMo-boric (A-C) (A) Ni $2p_{3/2}$ (B) Mo $3d_{3/2-5/2}$ (C) O 1s. And the XPS spectra of NiMo-Boric after HER at -1A cm^{-2} (D-E) (D) Ni $2p_{3/2}$ (E) Mo $3d_{3/2-5/2}$ (F) O 1s

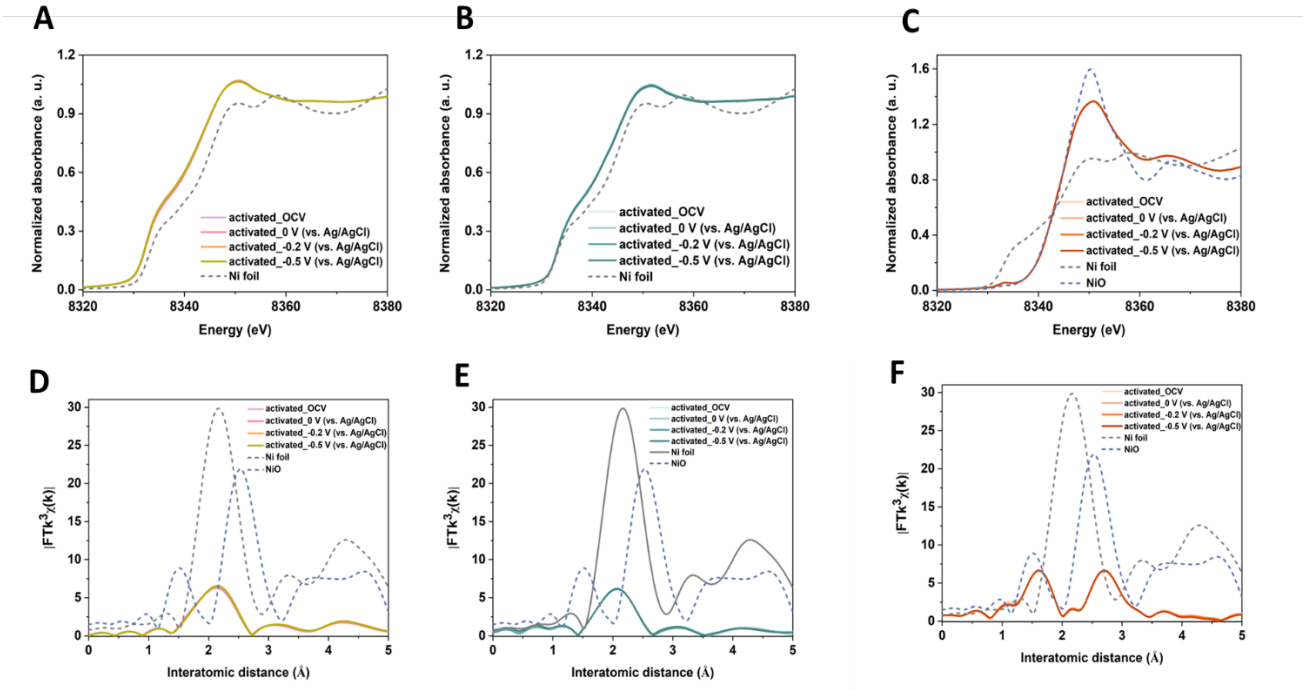

Figure S30. ***Operando* XAS data :** (A-C)-Ni K-edge XANES spectra of A- NiMo-AS1; B-NiMo-citric; C- NiMo-boric; (D-F)- Ni K-edge k^3-weighted EXAFS spectra for D-NiMo-AS1; E-NiMo-citric; F-NiMo-boric that underwent activation at various applied potentials in 1.0 M KOH.

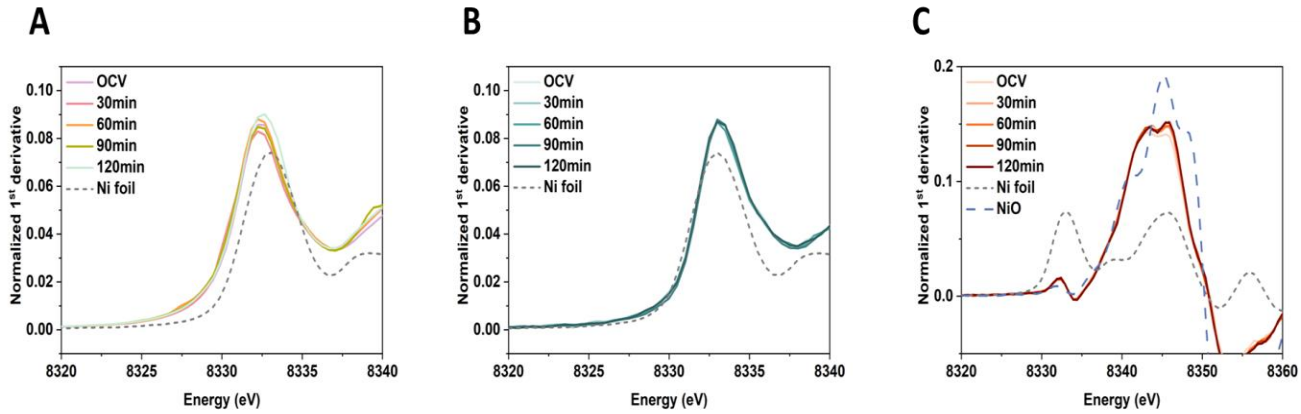

Figure S31. ***Operando* XAS data :** (A-C)-First derivatives of the Ni K-edge XANES spectra of A- NiMo-AS1; B- NiMo-citric; C- NiMo-boric during activation in 1.0 M KOH.

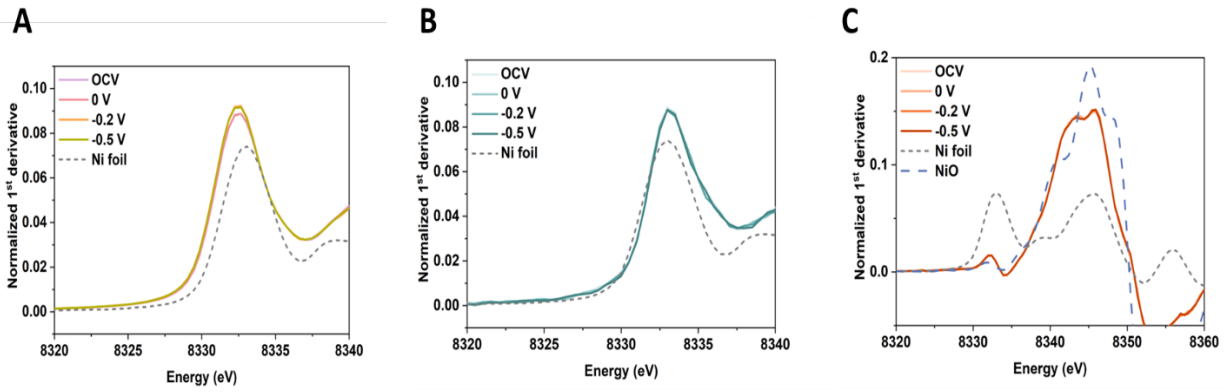

Figure S32. ***Operando* XAS data :** (A-C)-First derivatives of the Ni K-edge XANES spectra of A- NiMo-AS1; B- NiMo-citric; C- NiMo-boric that underwent activation at various applied potentials in 1.0 M KOH.

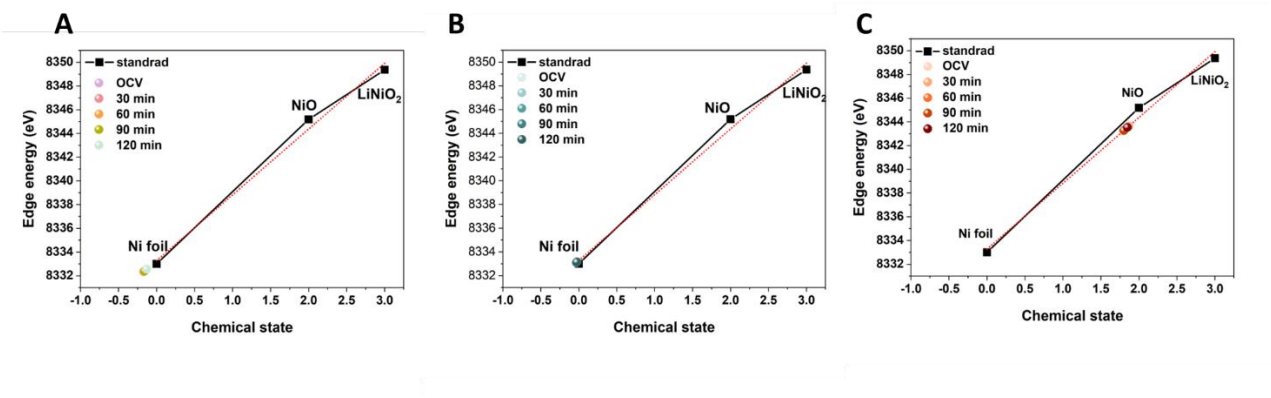

Figure S33. ***Operando* XAS data:** (A-C)-The chemical state of the Ni sites of A- NiMo-AS1; B- NiMo-citric; C- NiMo-boric during activation in 1.0 M KOH.

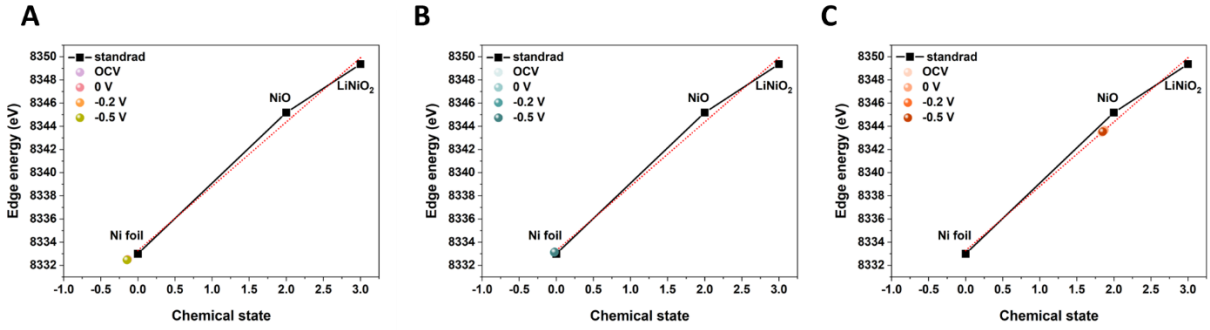

Figure S34. ***Operando* XAS data:** (A-C) the chemical state of the Ni sites of A- NiMo-AS1; B- NiMo-citric; C- NiMo-boric that underwent activation at various applied potentials in 1.0 M KOH.

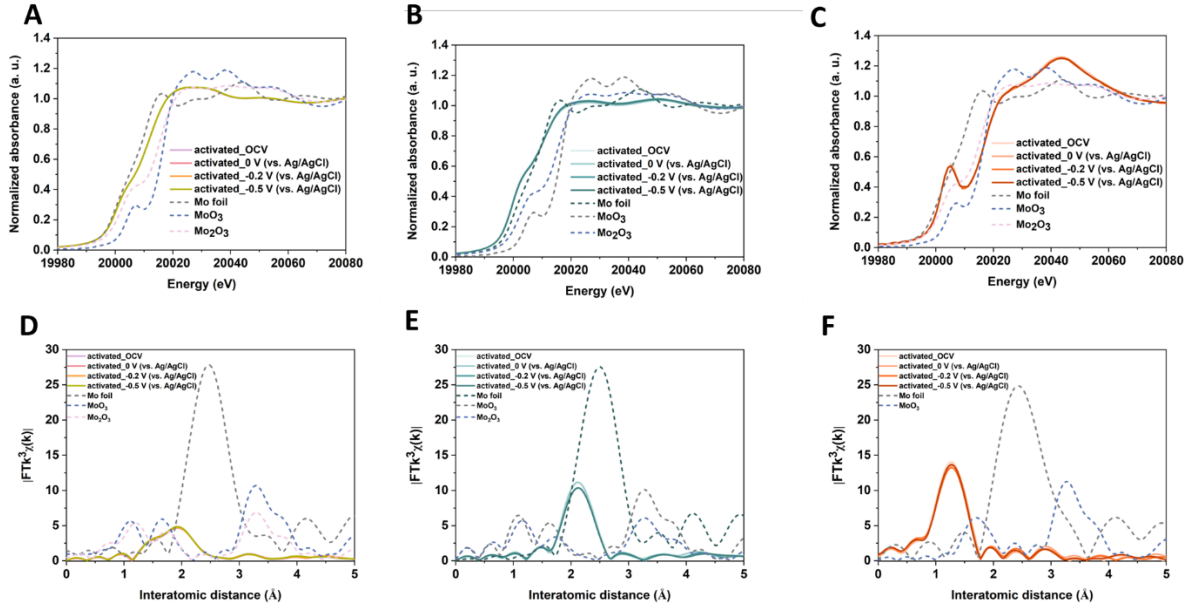

Figure S35. ***Operando* XAS data.** (A-C) Mo K-edge XANES spectra of A- NiMo-AS1; B- NiMo-citric; C- NiMo-boric; (D-F) Mo K-edge k3-weighted EXAFS spectra for D-NiMo-AS1, E-NiMo-citric, and F-NiMo-boric that underwent activation at various applied potentials in 1.0 M KOH.

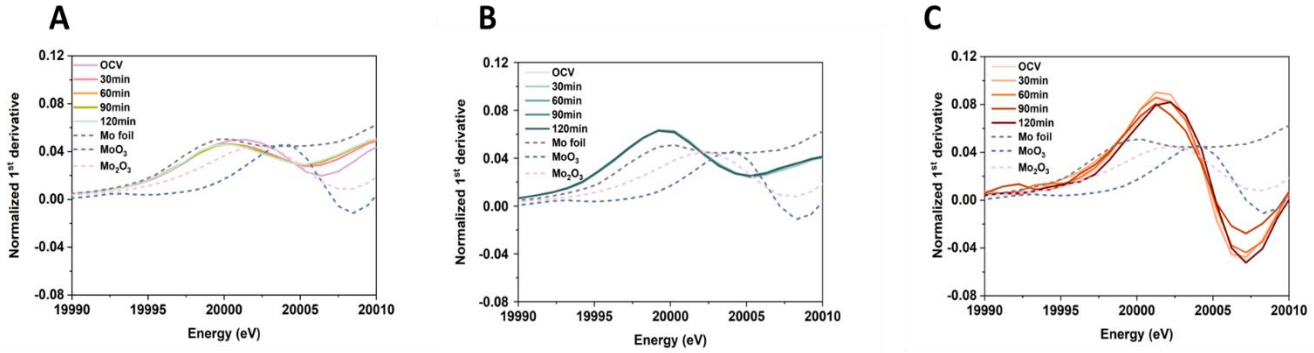

Figure S36. ***Operando* XAS data.** (A-C)-First derivatives of the Mo K-edge XANES spectra of A- NiMo-AS1; B- NiMo-citric; C- NiMo-boric during activation in 1.0 M KOH.

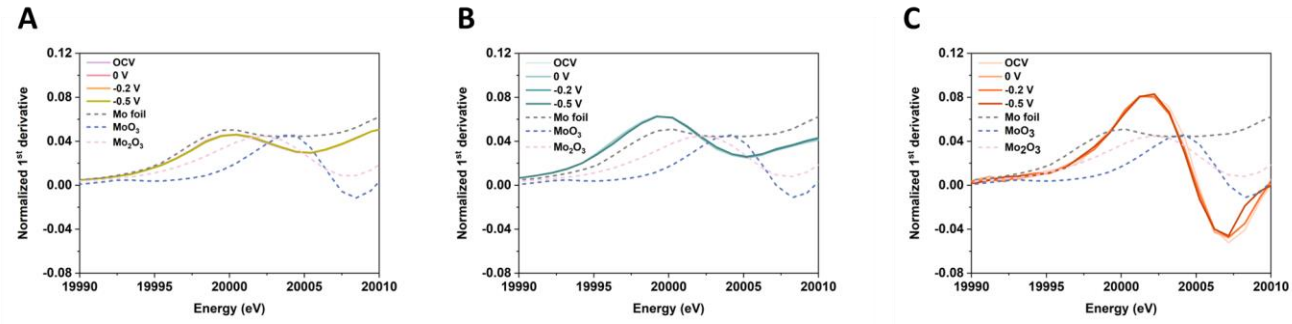

Figure S37. ***Operando* XAS data.** (A-C)-First derivatives of the Mo K-edge XANES spectra of A- NiMo-AS1; B- NiMo-citric; C- NiMo-boric that underwent activation at various applied potentials in 1.0 M KOH.

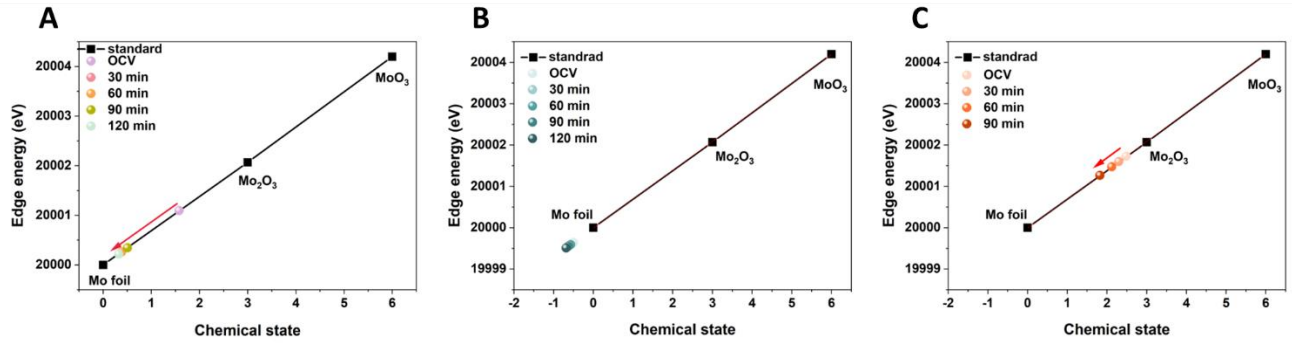

Figure S38. ***Operando* XAS data.** (A-C)-The chemical state of the Mo sites of A- NiMo-AS1; B- NiMo-citric; C- NiMo-boric during activation in 1.0 M KOH.

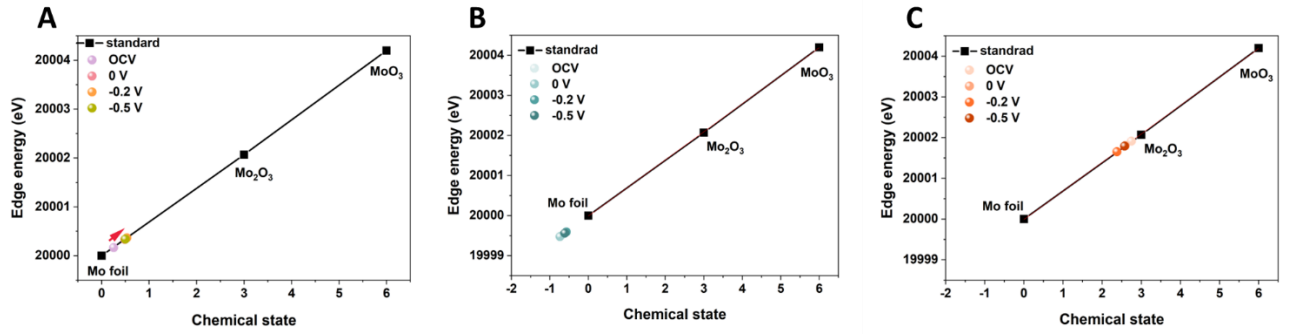

Figure S39. ***Operando* XAS data.** (A-C)-the chemical state of the Mo sites of A- NiMo-AS1; B- NiMo-citric; C- NiMo-boric that underwent activation at various applied potentials in 1.0 M KOH.

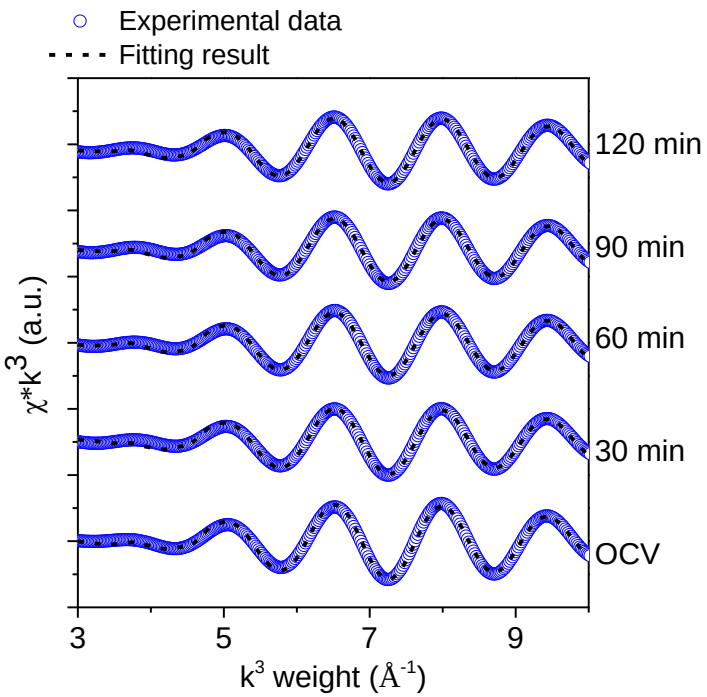

Figure S40. **EXAFS fitting curves in k-space.** Fitting results of *operando* k-space Ni K-edge EXAFS spectra of NiMo-AS1 during activation in 1.0 M KOH. Fitting structural parameters are gathered in Table S5.

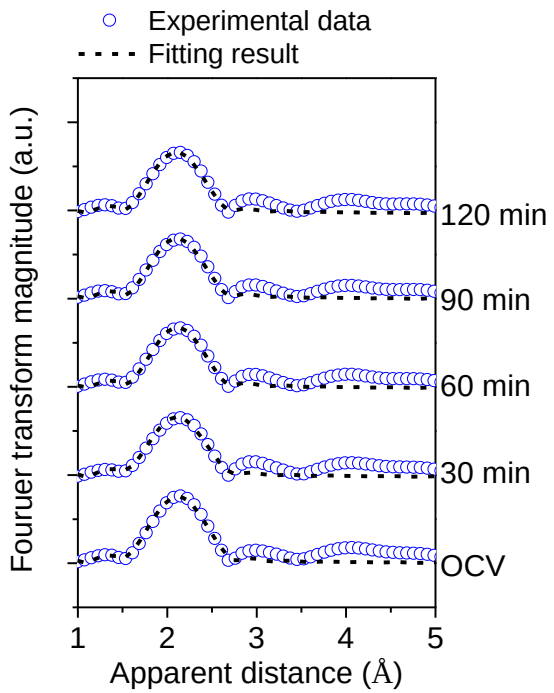

Figure S41. **EXAFS fitting curves in R-space.** Fitting results of *operando* R-space Ni K-edge EXAFS spectra of NiMo-AS1 during activation in 1.0 M KOH. Fitting structural parameters are gathered in Table S5.

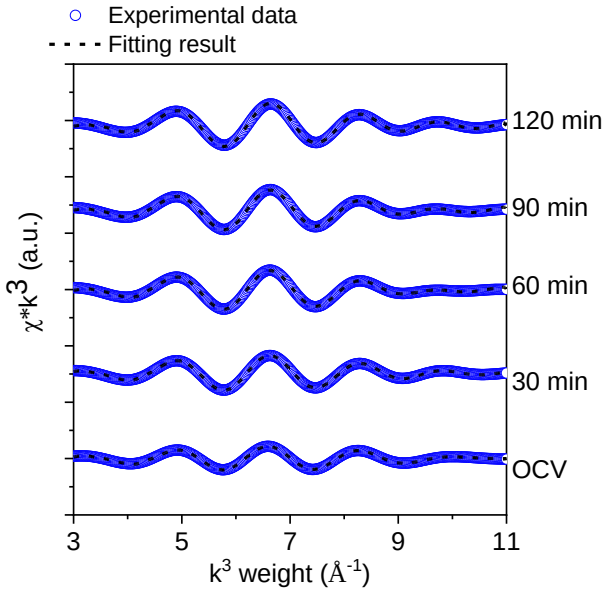

Figure S42. **EXAFS fitting curves in k-space.** Fitting results of *operando* k-space Mo K-edge EXAFS spectra of NiMo-AS1 during activation in 1.0 M KOH. Fitting structural parameters are gathered in Table S6.

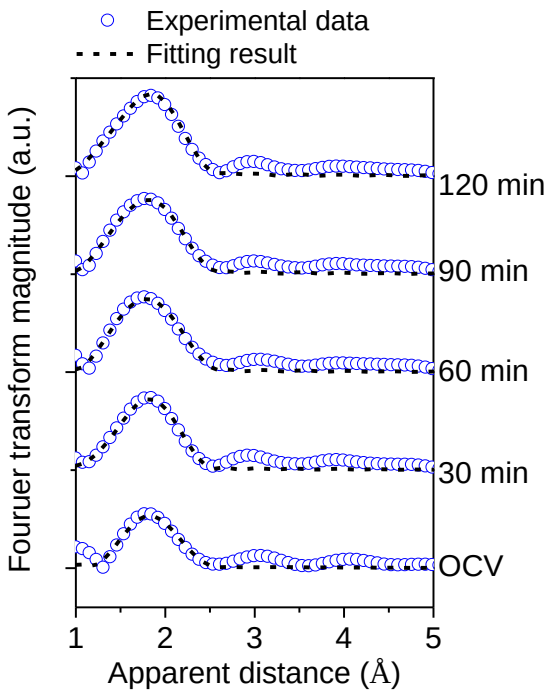

Figure S43. **EXAFS fitting curves in R-space.** Fitting results of *operando* R-space Mo K-edge EXAFS spectra of NiMo-AS1 during activation in 1.0 M KOH. Fitting structural parameters are gathered in Table S6.

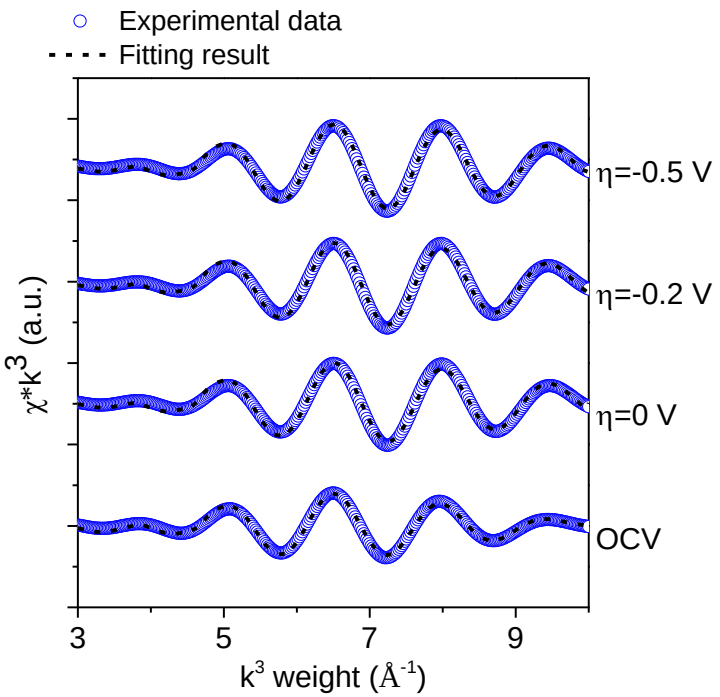

Figure S44. **EXAFS fitting curves in k-space.** Fitting results of *operando* k-space Ni K-edge EXAFS spectra of NiMo-AS1 that underwent activation at various applied potentials in 1.0 M KOH. Fitting structural parameters are gathered in Table S7.

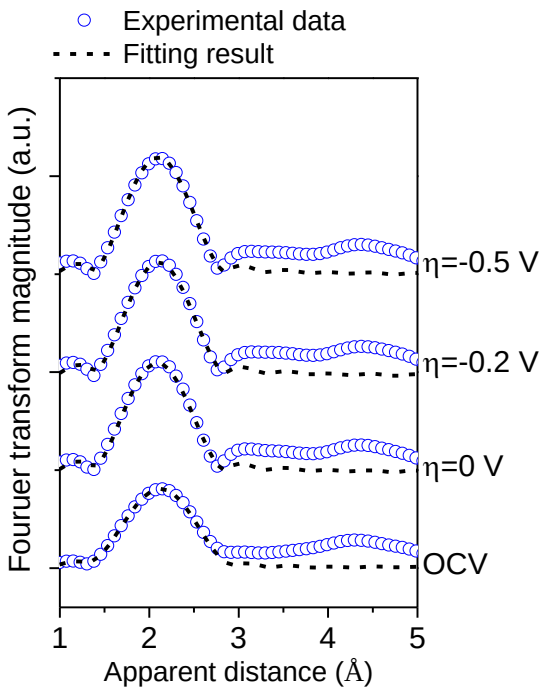

Figure S45. **EXAFS fitting curves in R-space.** Fitting results of *operando* R-space Ni K-edge EXAFS spectra of NiMo-AS1 that underwent activation at various applied potentials in 1.0 M KOH. Fitting structural parameters are gathered in Table S7.

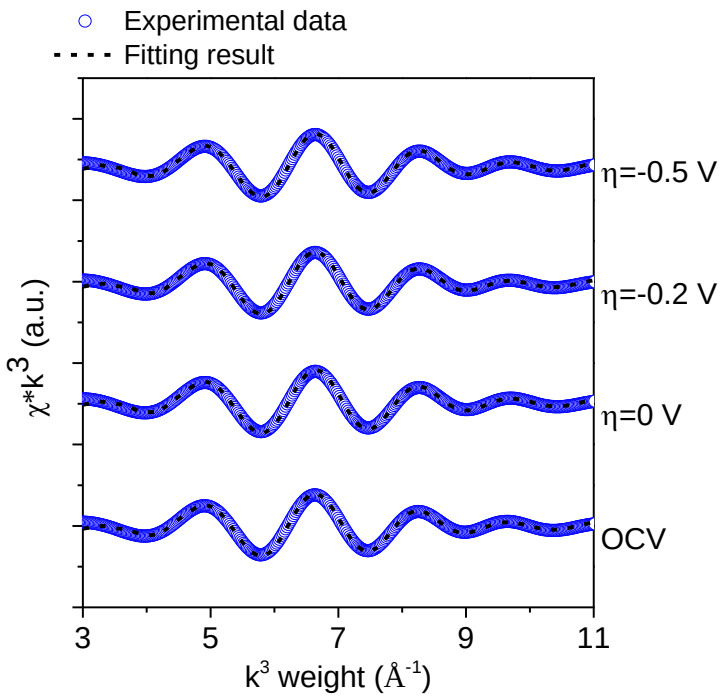

Figure S46. **EXAFS fitting curves in k-space.** Fitting results of *operando* k-space Mo K-edge EXAFS spectra of NiMo-AS1 that underwent activation at various applied potentials in 1.0 M KOH. Fitting structural parameters are gathered in Table S8.

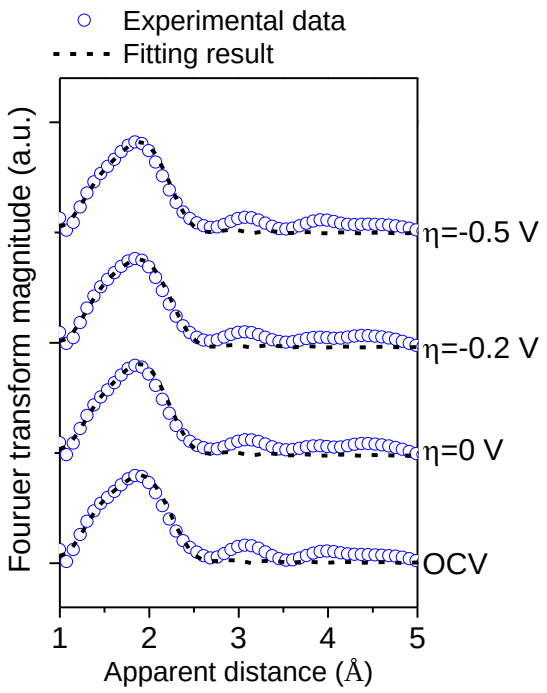

Figure S47. **EXAFS fitting curves in R-space.** Fitting results of *operando* R-space Mo K-edge EXAFS spectra of NiMo-AS1 that underwent activation at various applied potentials in 1.0 M KOH. Fitting structural parameters are gathered in Table S8.

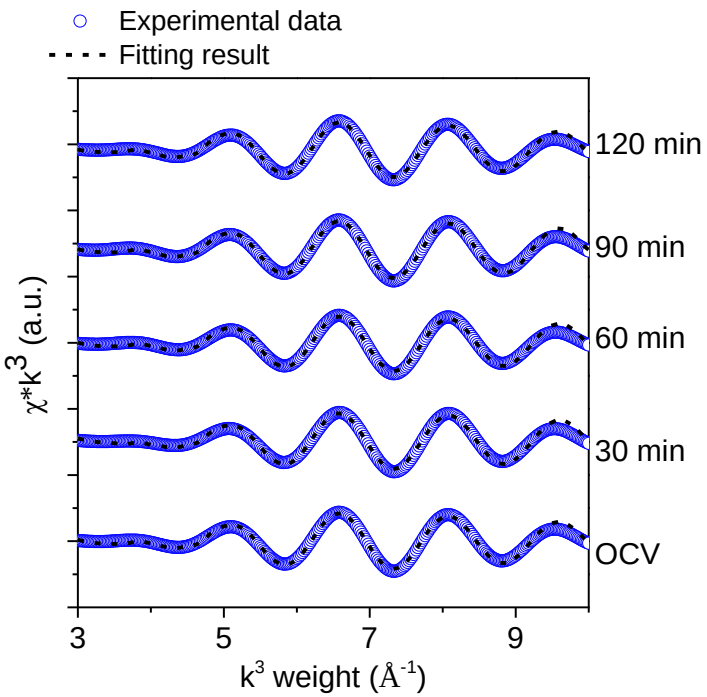

Figure S48. **EXAFS fitting curves in k-space.** Fitting results of *operando* k-space Ni K-edge EXAFS spectra of NiMo-citric during activation in 1.0 M KOH. Fitting structural parameters are gathered in Table S9.

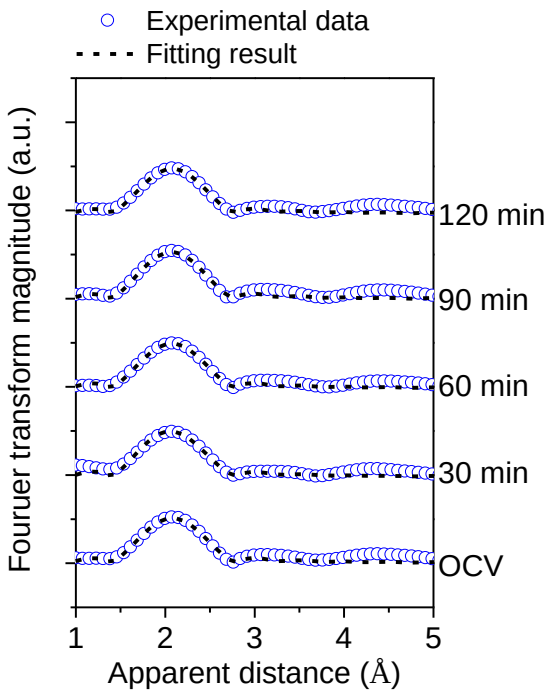

Figure S49. **EXAFS fitting curves in R-space.** Fitting results of *operando* k-space Ni K-edge EXAFS spectra of NiMo-citric during activation in 1.0 M KOH. Fitting structural parameters are gathered in Table S9.

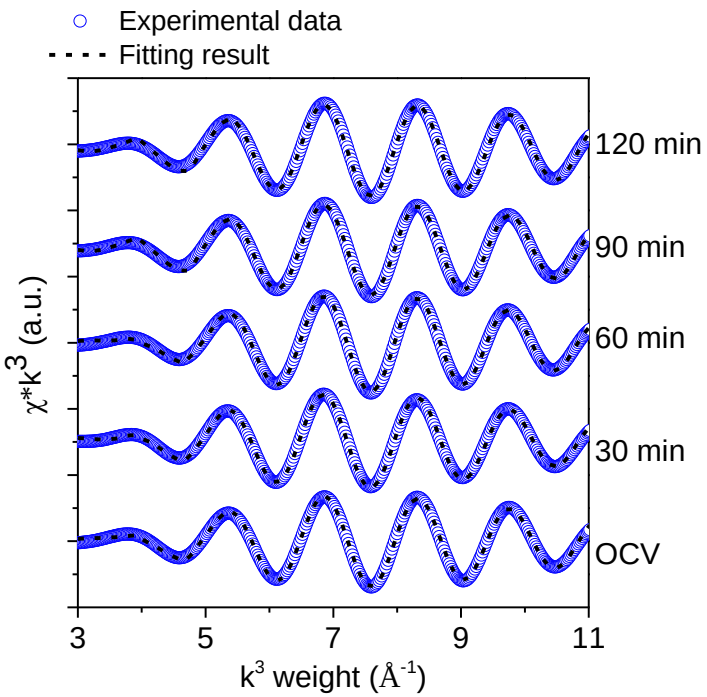

Figure S50. **EXAFS fitting curves in k-space.** Fitting results of *operando* k-space Mo K-edge EXAFS spectra of NiMo-citric during activation in 1.0 M KOH. Fitting structural parameters are gathered in Table S10

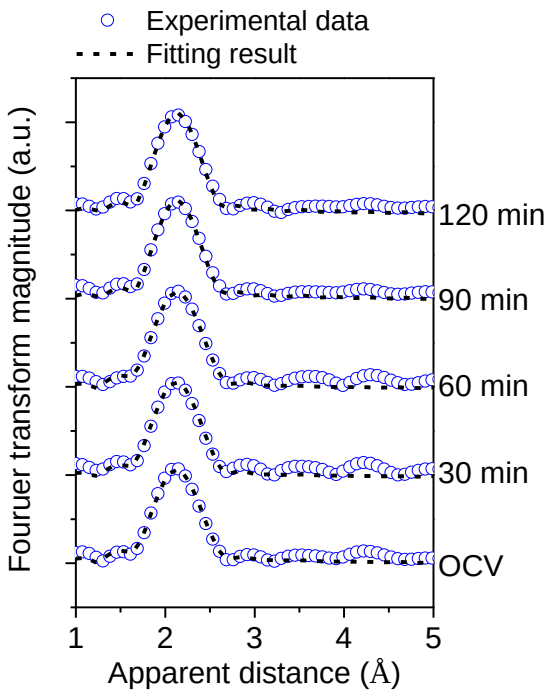

Figure S51. **EXAFS fitting curves in R-space.** Fitting results of *operando* k-space Mo K-edge EXAFS spectra of NiMo-citric during activation in 1.0 M KOH. Fitting structural parameters are gathered in Table S10.

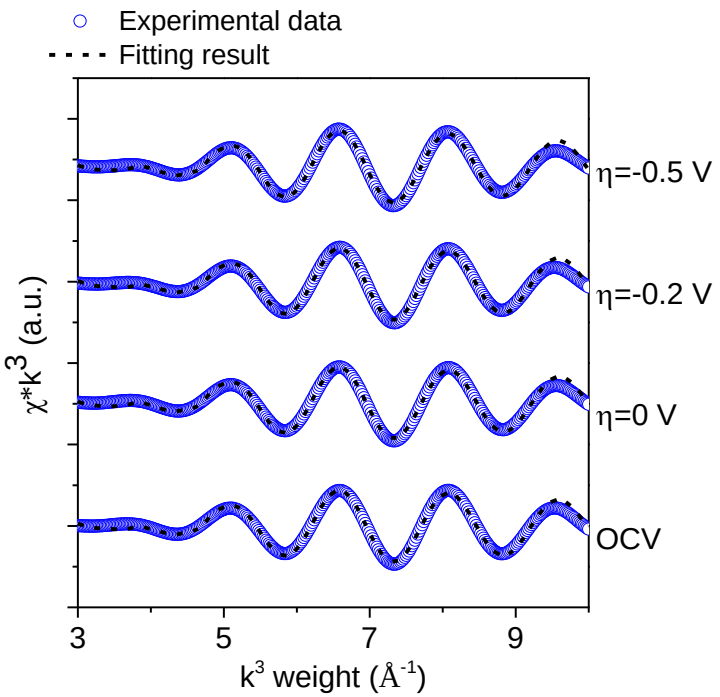

Figure S52. **EXAFS fitting curves in k-space.** Fitting results of *operando* k-space Ni K-edge EXAFS spectra of NiMo-citric that underwent activation at various applied potentials in 1.0 M KOH. Fitting structural parameters are gathered in Table S11.

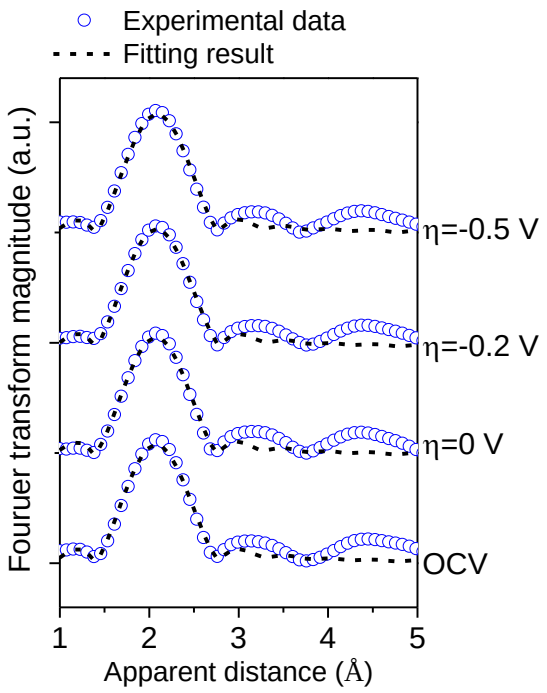

Figure S53. **EXAFS fitting curves in R-space.** Fitting results of *operando* k-space Ni K-edge EXAFS spectra of NiMo-citric that underwent activation at various applied potentials in 1.0 M KOH. Fitting structural parameters are gathered in Table S11.

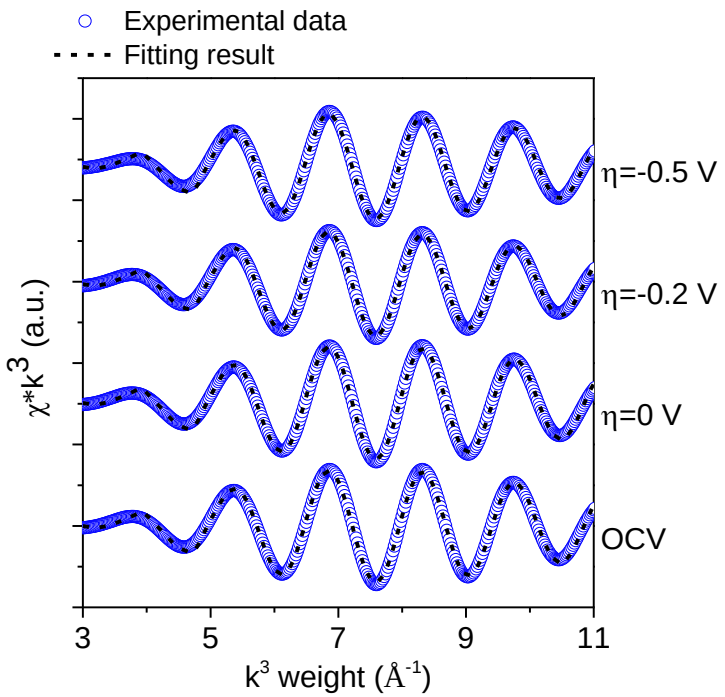

Figure S54. **EXAFS fitting curves in k-space.** Fitting results of *operando* k-space Mo K-edge EXAFS spectra of NiMo-citric that underwent activation at various applied potentials in 1.0 M KOH. Fitting structural parameters are gathered in Table S12.

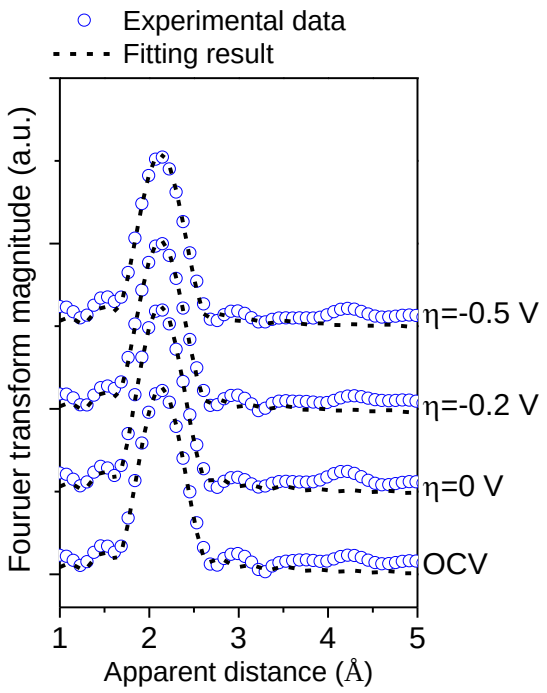

Figure S55. **EXAFS fitting curves in R-space.** Fitting results of *operando* k-space Mo K-edge EXAFS spectra of NiMo-citric that underwent activation at various applied potentials in 1.0 M KOH. Fitting structural parameters are gathered in Table S12.

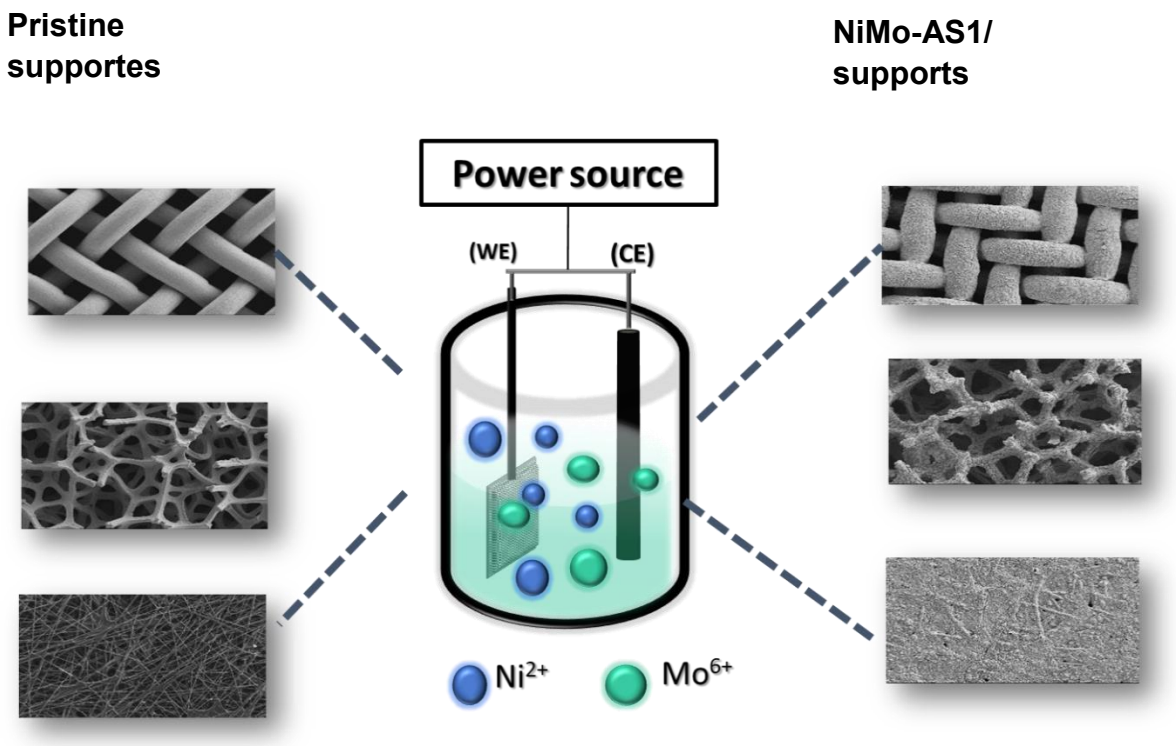

Fig.S56. A scheme of the electrodeposition bath.

Material	C_s values ($uF\ cm^{-2}$)
Ni	25
Pt	28
Pt/C	30

Tabel S1. Values of specific capacitance (Cs) of bare Nickel, Platinum and Pt /C

The values of the Cs were taken from a previously reported work.[20]

Support	ESCA/ (cm^2) NiMo-AS1 AA	ESCA/ (cm^2) NiMo-citric AA	ESCA/ (cm^2) NiMo-boric AA	ESCA/ (cm^2) Pt/C	ESCA/ (cm^2) Ni mesh AA	ESCA/ (cm^2) Pt mesh AA
C paper	2.76	3.22	1.6	2.28		
Mesh	3.2	5.04	2.6	x	1.44	1.78

Tabel S2. Values of the electrochemically active surface area of the NiMo-AS1, NiMo-citric, NiMo-boric, Pt/C, Ni mesh, and Pt mesh.

The values of the ESCA were calculated using the formula:

$$ESCA=C_{dl}/C_s$$

The Cdl values were calculated using the formula:

$$2C_{dl}\ (Slope)=\Delta j$$

For consistency, Δj was measured at just one point in all cyclic voltammetries; at 0.21V vs. RHE

Support	NiMo-AS1 (mg cm^{-2})	NiMo-citric (mg cm^{-2})	NiMo-boric (mg cm^{-2})
Ni mesh	32	26	17
Carbon paper	30	24	15

Tabel S3. Catalysts loadings for NiMo-AS1, NiMo-citric, and NiMo-boric on both C and Ni support.

Ni as prepared (ug/mg)	Average	Mo as prepared (ug/mg)	Average	Ni after activ. (ug/mg)	Average	Mo after activ.(ug/mg)	Average
334.73	355.46	194.26	168.65	361.19	351.1366667	136.2	134.65
353.2	St deviation	144.59	St deviation	340.25	St deviation	128.19	St deviation
378.45	21.94	167.1	24.87	351.97	10.49	139.56	5.84
	St error		St error		St error		St error
	12.67		14.35		6.05		3.37
	Ni /Atomic mass		Mo/Atomic mass		Ni /Atomic mass		Mo/Atomic mass
	6.05		1.75		5.98		1.41
		Ratio Ni/Mo as prep				Ratio Ni/Mo after activ	
		3.446				4.21	

Table S4. ICP-results and calculation.

sample	path	R	N	dE	DW	R-factor
OCV	Ni-Ni	2.48(1)	2.9(1)	-0.0(4)	0.044(6)	1.204
	Ni-Mo	2.46(1)	1.1(1)	-17.0(11)	0.028(19)	
30 min	Ni-Ni	2.46(1)	2.8(1)	-1.3(4)	0.052(5)	2.085
	Ni-Mo	2.44(2)	1.0(1)	-16.0(4)	0.041(16)	
60 min	Ni-Ni	2.46(1)	2.8(2)	-1.1(6)	0.074(6)	2.694
	Ni-Mo	2.46(2)	1.0(2)	-18.3(8)	0.086(18)	
90 min	Ni-Ni	2.46(1)	2.7(1)	-1.4(6)	0.067(5)	2.929
	Ni-Mo	2.46(2)	1.0(2)	-17.7(7)	0.073(16)	
120 min	Ni-Ni	2.47(1)	2.6(1)	-1.7(5)	0.060(6)	2.205
	Ni-Mo	2.46(2)	0.9(1)	-18.2(5)	0.056(17)	

Table S5. Structural parameters of NiMo-AS1 extracted from *operando* Ni K-edge EXAFS refinement during activation in 1.0 M KOH.

sample	path	R	N	dE	DW	R-factor
OCV	Mo-Ni	2.46(1)	2.5(4)	-18.2(19)	0.126(13)	0.129
	Mo-O	2.03(5)	0.5(3)	-19.3(161)	0.043(94)	
30 min	Mo-Ni	2.44(2)	3.0(9)	-20.2(39)	0.117(27)	0.139
	Mo-O	1.98(5)	1.0(9)	-22.3(124)	0.08(86)	
60 min	Mo-Ni	2.46(2)	3.1(8)	-16.9(33)	0.118(22)	0.569
	Mo-O	1.98(3)	1.1(5)	-20.1(85)	0.057(61)	
90 min	Mo-Ni	2.46(2)	3.0(7)	-17.5(34)	0.115(20)	0.466
	Mo-O	1.97(3)	1.1(6)	-21.0(87)	0.064(60)	
120 min	Mo-Ni	2.46(2)	3.1(6)	-17.8(31)	0.111(19)	0.572
	Mo-O	1.96(1)	1.5(8)	-21.8(75)	0.083(50)	

Table S6. Structural parameters of NiMo-AS1 extracted from *operando* Mo K-edge EXAFS refinement during activation in 1.0 M KOH.

sample	path	R	N	dE	DW	R-factor
OCV	Ni-Ni	2.51(1)	3.1(1)	2.7(7)	0.079(12)	1.888
	Ni-Mo	2.47(2)	1.4(1)	-17.7(16)	0.059(20)	
η= 0 V	Ni-Ni	2.49(1)	3.0(1)	-0.1(7)	0.063(15)	2.576
	Ni-Mo	2.46(2)	1.3(1)	-18.0(17)	0.048(29)	
η= -0.2 V	Ni-Ni	2.49(1)	3.0(1)	0.7(7)	0.060(15)	2.205
	Ni-Mo	2.47(2)	1.3(1)	-17.5(17)	0.042(31)	
η= -0.5 V	Ni-Ni	2.49(1)	2.9(1)	0.4(7)	0.054(16)	2.108
	Ni-Mo	2.46(2)	1.3(1)	-18.1(17)	0.029(42)	

Table S7. Structural parameters of NiMo-AS1 that underwent activation extracted from *operando* Ni K-edge EXAFS refinement at various applied potentials in 1.0 M KOH.

sample	path	R	N	dE	DW	R-factor
OCV	Mo-Ni	2.47(2)	3.2(5)	-15.8(30)	0.115(13)	1.321
	Mo-O	1.97(3)	1.6(7)	-21.0(71)	0.087(36)	
η= 0 V	Mo-Ni	2.46(2)	3.3(6)	-16.5(31)	0.116(14)	1.152
	Mo-O	1.97(3)	1.7(8)	-21.3(73)	0.093(38)	
η= -0.2 V	Mo-Ni	2.47(2)	3.3(6)	-15.9(31)	0.117(14)	1.101
	Mo-O	1.97(3)	1.6(7)	-20.4(74)	0.086(36)	
η= -0.5 V	Mo-Ni	2.46(2)	3.4(6)	-16.2(30)	0.115(14)	1.233
	Mo-O	1.97(3)	1.7(7)	-20.8(72)	0.090(36)	

Table S8. Structural parameters of NiMo-AS1 that underwent activation extracted from *operando* Mo K-edge EXAFS refinement at various applied potentials in 1.0 M KOH.

sample	path	R	N	dE	DW	R-factor
OCV	Ni-Ni	2.48(1)	3.2(1)	2.7(6)	0.096(8)	2.621
	Ni-Mo	2.51(1)	1.3(2)	-12.1(20)	0.066(7)	
30 min	Ni-Ni	2.48(1)	3.2(1)	2.3(17)	0.092(12)	4.067
	Ni-Mo	2.51(1)	1.2(2)	-10.7(23)	0.059(23)	
60 min	Ni-Ni	2.48(1)	3.2(1)	2.5(15)	0.098(10)	3.367
	Ni-Mo	2.52(1)	1.2(1)	-12.1(21)	0.063(19)	
90 min	Ni-Ni	2.48(1)	3.3(1)	1.8(15)	0.099(10)	2.866
	Ni-Mo	2.52(1)	1.2(1)	-13.1(21)	0.063(18)	
120 min	Ni-Ni	2.47(1)	3.3(1)	1.2(14)	0.101(8)	2.670
	Ni-Mo	2.52(1)	1.2(1)	-13.0(21)	0.076(18)	

Table S9. Structural parameters of NiMo-citric extracted from *operando* Ni K-edge EXAFS refinement during activation in 1.0 M KOH.

sample	path	R	N	dE	DW	R-factor
OCV	Mo-Ni	2.52(1)	4.0(2)	1.7(7)	0.082(8)	1.101
	Mo-Mo	2.63(2)	1.9(5)	-5.4(30)	0.113(33)	
30 min	Mo-Ni	2.51(2)	3.8(5)	0.1(13)	0.084(10)	0.989
	Mo-Mo	2.66(7)	2.0(13)	-7.4(53)	0.110(59)	
60 min	Mo-Ni	2.51(1)	3.9(3)	0.0(3)	0.087(9)	0.682
	Mo-Mo	2.67(2)	2.0(5)	-5.3(10)	0.097(19)	
90 min	Mo-Ni	2.52(1)	4.4(4)	0.9(9)	0.099(22)	1.253
	Mo-Mo	2.64(1)	2.2(6)	-8.8(26)	0.082(14)	
120 min	Mo-Ni	2.52(1)	4.0(3)	1.5(7)	0.083(25)	1.182
	Mo-Mo	2.64(3)	2.1(8)	-6.4(32)	0.101(65)	

Table S10. Structural parameters of NiMo-citric extracted from *operando* Mo K-edge EXAFS refinement during activation in 1.0 M KOH.

sample	path	R	N	dE	DW	R-factor
OCV	Ni-Ni	2.48(1)	3.3(1)	2.8(15)	0.095(10)	2.389
	Ni-Mo	2.52(1)	1.3(1)	-11.4(20)	0.063(20)	
η= 0 V	Ni-Ni	2.48(1)	3.3(1)	2.5(5)	0.096(8)	2.502
	Ni-Mo	2.51(1)	1.3(2)	-12.8(19)	0.062(7)	
η= -0.2 V	Ni-Ni	2.49(1)	3.3(1)	3.6(5)	0.092(8)	2.861
	Ni-Mo	2.52(1)	1.3(2)	-10.9(19)	0.060(8)	
η= -0.5 V	Ni-Ni	2.49(1)	3.3(3)	3.4(8)	0.095(8)	2.779
	Ni-Mo	2.52(1)	1.3(2)	-12.2(5)	0.062(19)	

Table S11. Structural parameters of NiMo-citric that underwent activation extracted from *operando* Ni K-edge EXAFS refinement at various applied potentials in 1.0 M KOH.

sample	path	R	N	dE	DW	R-factor
OCV	Mo-Ni	2.52(1)	3.9(3)	1.2(7)	0.084(21)	1.100
	Mo-Mo	2.64(2)	2.0(7)	-6.8(32)	0.098(51)	
η= 0 V	Mo-Ni	2.52(1)	4.2(2)	1.4(7)	0.087(11)	1.408
	Mo-Mo	2.63(1)	1.9(5)	-6.8(28)	0.093(21)	
η= -0.2 V	Mo-Ni	2.52(1)	4.1(5)	1.2(8)	0.094(26)	0.920
	Mo-Mo	2.64(2)	2.0(6)	-7.4(29)	0.092(33)	
η= -0.5 V	Mo-Ni	2.52(1)	4.3(4)	0.9(8)	0.097(23)	1.062
	Mo-Mo	2.64(1)	2.2(6)	-8.0(27)	0.091(23)	

Table S12. Structural parameters of NiMo-citric that underwent activation extracted from *operando* Mo K-edge EXAFS refinement at various applied potentials in 1.0 M KOH

Referenes

[1] Cao, Jun, et al. "Hierarchical NiMo alloy microtubes on nickel foam as an efficient electrocatalyst for hydrogen evolution reaction." *Int. J. Hydrogen Energy* 2019, 44-45, 24712-24718.

[2] Zhao, Meng-Jie, et al. "Green Synthesis of a Ni-Mo-O Composite Catalyst for Superior Hydrogen Production in Acidic and Alkaline Electrolytes." SSRN Electronic Journal, DOI:10.2139/ssrn.3996127.

[3] Chen, Yudan, et al. "Macroporous NiMo alloy Self-Supporting Electrode for Efficient Hydrogen Evolution at Ultrahigh Current Densities." *Mater. Adv.,* 2023,4, 2868-2873

[4] Mao, Fangxin, et al. "Electrodeposited Multimetal Alloyed NiMoCo on Ni Mesh for Efficient Alkaline Hydrogen Evolution Reaction." *Energy & Fuels* 2023, 37, 18137-18144.

[9] L. Wang, Y. Hao, L. Deng, F. Hu, S. Zhao, L. Li and S. Peng, Rapid complete reconfiguration induced actual active species for industrial hydrogen evolution reaction, *Nat. Commun.*, 2022, **13**, 5785

[10] Mishra, I. K.; Zhou, H.; Sun, J.; Qin, F.; Dahal, K.; Bao, J.; Chen, S.; Ren, Z. Hierarchical CoP/Ni5P4/CoP Microsheet Arrays as a Robust Ph-Universal Electrocatalyst for Efficient Hydrogen Generation. Energy Environ. Sci. 2018, 11, 2246−2252

[11]Yu, P.; Wang, F.; Shifa, T. A.; Zhan, X.; Lou, X.; Xia, F.; He, J. Earth Abundant Materials Beyond Transition Metal Dichalcogenides: A Focus on Electro-catalyzing Hydrogen Evolution Reaction. Nano Energy. 2019, 58, 244−276

[12] Yang, H.; Chen, Z.; Guo, P.; Fei, B.; Wu, R. B-Doping-Induced Amorphization of Ldh for Large-Current-Density Hydrogen Evolution Reaction. Appl. Catal., B 2020, 261, 118240

[13] Ren, B.; Li, D.; Jin, Q.; Cui, H.; Wang, C. Integrated 3D SelfSupported Ni Decorated MoO2 Nanowires as Highly Efficient Electrocatalysts for Ultra-Highly Stable and Large-Current-Density Hydrogen Evolution. J. Mater. Chem. A 2017, 5, 24453−24461

[14] Hao, W.; Wu, R.; Huang, H.; Ou, X.; Wang, L.; Sun, D.; Ma, X.; Guo, Y. Fabrication of Practical Catalytic Electrodes Using Insulating and Eco-Friendly Substratesfor Overall Water Splitting. Energy Environ. Sci. 2020, 13, 102−110

[15] Huang, C.; Yu, L.; Zhang, W.; Xiao, Q.; Zhou, J.; Zhang, Y.; An, P.; Zhang, J.; Yu, Y. N-Doped Ni-Mo Based Sulfides for High-Efficiency and Stable Hydrogen Evolution Reaction. Appl. Catal., B 2020, 276, 119137

[16] Qian, G.; Yu, G.; Lu, J.; Luo, L.; Wang, T.; Zhang, C.; Ku, R.; Yin, S.; Chen, W.; Mu, S. Ultra-Thin N-Doped-Graphene Encapsulated Ni Nanoparticles Coupled with MoO2 Nanosheets for Highly Efficient Water Splitting at Large Current Density. J. Mater. Chem. A 2020, 8, 14545−1554

[17] Yu, L.; Mishra, I. K.; Xie, Y.; Zhou, H.; Sun, J.; Zhou, J.; Ni, Y.; Luo, D.; Yu, F.; Yu, Y.; Chen, S.; Ren, Z. Ternary Ni2(1-x)Mo2xP Nanowire Arrays toward Efficient and Stable Hydrogen Evolution Electrocatalysis under Large-Current-Density. Nano Energy. 2018, 53, 492−500.

[18] Wang, Y.; Qian, G.; Xu, Q.; Zhang, H.; Shen, F.; Luo, L.; Yin, S. Industrially Promising IrNi-FeNi3 Hybrid Nanosheets for Overall Water Splitting Catalysis at LargeCurrent Density. Appl. Catal., B 2021, 286, 119881.

[19] H. Yang, Z. Chen, P. Guo, B. Fei and R. Wu, B-doping-induced amorphization of LDH for large-current-density hydrogen evolution reaction, Appl. Catal., B, 2020, 261, 118240

[20] McCrory, Charles CL, et al. "Benchmarking heterogeneous electrocatalysts for the oxygen evolution reaction." *J. Am. Chem. Soc.* 2013*,* 135, 16977-16987.